Environmental Science: Atmospheres

ROYAL SOCIETY OF CHEMISTRY

PAPER

View Article Online
View Journal

Cite this: DOI: 10.1039/d5ea00091b

Comparison of oxidation products generated from the reaction of α-pinene with hydroxyl radicals, chlorine atoms, and bromine atoms measured using ammonium adduct chemical ionization mass spectrometry

Andrew T. Lambe, *[a] Jordan E. Krechmer,†[a] Anita M. Avery, [a] Mitchell W. Alton, [a] Neil M. Donahue [b] and Manjula R. Canagaratna[a]

Halogen atoms play important but undercharacterized roles in atmospheric oxidation chemistry. Here, we report laboratory measurements of gas- and condensed-phase products formed from the oxidation of α-pinene by hydroxyl radicals (OH), chlorine atoms (Cl), and bromine atoms (Br) in an oxidation flow reactor (OFR). Products were detected using a Vocus proton-transfer time-of-flight reaction mass spectrometer (PTR-ToF-MS) operated with low-pressure ammonium adduct (NH_4^+) ionization and a Vaporization Inlet for Aerosols (VIA). We applied Positive Matrix Factorization (PMF) to classify precursor and product ions into early and later-generation oxidation products. While some common products were observed across all oxidants, significant compositional differences were also apparent. Vocus : VIA signal ratios were used to estimate volatility trends, revealing that more highly oxygenated compounds and many halogenated products contributed to SOA formation. Cl and Br oxidation led to the formation of oxygenated volatile organic compounds (OVOCs) and secondary organic aerosol (SOA), which retained halogen atoms, with Br-derived products exhibiting the lowest carbon oxidation state and the highest halogen retention. Halogenated oxidation products were less volatile than their non-halogenated counterparts. Photochemical modeling suggests that the fates of organic peroxy radicals (RO_2) were primarily influenced by RO_2 + HO_2 reactions for α-pinene/OH, RO_2 + Cl, RO_2 + HO_2, and potentially RO_2 isomerization/autooxidation reactions for α-pinene/Cl, and RO_2 + Br reactions for α-pinene/Br.

Received 4th August 2025
Accepted 6th January 2026

DOI: 10.1039/d5ea00091b

rsc.li/esatmospheres

Environmental significance

Chlorine (Cl) and bromine (Br) atoms are increasingly recognized as important atmospheric oxidants, especially in coastal, marine, and polar environments. This study provides a comprehensive molecular-level comparison of products generated from the oxidation of α-pinene by OH, Cl, and Br. Our analysis reveals distinct chemical pathways and product distributions for each oxidant. By identifying unique halogenated products and quantifying their volatility, this work highlights the need to account for halogen-specific chemistry in models. Our results contribute to an improved understanding of how halogen initiated oxidation of volatile organic compounds influences SOA formation and oxidative aging and support the development of more accurate atmospheric chemical mechanisms.

1 Introduction

Atmospheric oxidation processes play a central role in the transformation of organic and inorganic compounds, with gas-phase oxidants such as ozone (O_3), hydroxyl radicals (OH), nitrate radicals (NO_3), chlorine atoms (Cl), and bromine atoms (Br) initiating these reactions. The relative importance of these oxidants varies with regional meteorology, emissions, and photochemical conditions. Among them, OH is the most globally significant due to its rapid daytime production and its broad reactivity with atmospheric constituents. OH initiates key processes, including the oxidation of sulfur dioxide (SO_2) to sulfuric acid and the transformation of volatile organic compounds (VOCs) into low-volatility products that contribute to secondary organic aerosol (SOA) formation. While NO_3 dominates nighttime oxidation in certain regions, halogen atoms offer unique daytime oxidation pathways, especially in marine, polar, and urban atmospheres.[1,2] Cl is especially relevant in polluted coastal,[3–5] urban regions,[6,7] and other inland sources[8,9] and can

[a]Aerodyne Research, Billerica, Massachusetts, USA. E-mail: lambe@aerodyne.com
[b]Carnegie Mellon University Center for Atmospheric Particle Studies, Pittsburgh, Pennsylvania, USA
† 'Present address:' Osmo Labs, PBC, Somerville, Massachusetts, United States.

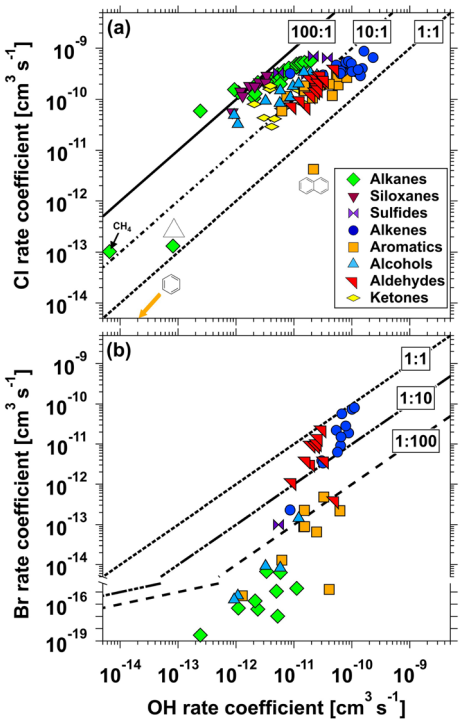

Fig. 1 Rate coefficients for reactions of (a) Cl and (b) Br *versus* OH with various classes of VOCs.[13–120] Solid and dashed lines indicate fixed ratios of halogen-to-OH reactivity: 100 : 1, 10 : 1, and 1 : 1 in (a), and 1 : 1, 1 : 10, and 1 : 100 in (b).

react with many VOCs with rate coefficients that are 10 to 100 times greater than OH (Fig. 1a). This reactivity is particularly enhanced for alkanes and siloxanes, where oxidation proceeds exclusively *via* hydrogen abstraction. Only a small subset of VOCs, such as benzene and naphthalene, exhibit lower reactivity toward Cl than OH. However, Cl does not significantly react with SO_2, limiting its role in sulfate aerosol formation. Br is especially active in the polar boundary layer,[10] where heterogeneous reactions on snow and ice surfaces release reactive bromine species that drive episodic O_3 depletion and oxidant cycling.[11,12] While Br is highly reactive with specific VOC classes such as alkenes and aldehydes, it is generally less reactive with alkanes, aromatics, and alcohols (Fig. 1b). Although Br has a high electron affinity, its H-abstraction reactions are typically endothermic, making them less favorable due to added reaction enthalpy and activation energy. Aldehydes are an exception: the formyl C–H bond is much weaker than other C–H bonds, making H-abstraction by Br nearly thermoneutral.

The role of Cl and Br in the oxidation of biogenic VOCs (BVOCs) has received far less attention than O_3, OH, and NO_3, particularly for α-pinene – a globally relevant BVOC often used as a model compound due to its well-characterized OH oxidation chemistry. α-Pinene reacts with Cl at near gas-kinetic rates[53,121] and with Br at a rate roughly half that of OH.[37] While early studies primarily focused on reaction kinetics, more recent work has begun to examine the chemical composition of SOA formed from Cl-and Br-initiated α-pinene oxidation. Cl-driven oxidation has been shown to generate highly oxygenated molecules – including chlorinated products – with SOA yields that are comparable to or greater than those from OH.[122–125] Far fewer studies have investigated Br-initiated α-pinene oxidation, but existing results indicate very low SOA yields.[125,126] These findings highlight the potential for halogen atoms to significantly alter SOA composition and yield in environments influenced by reactive halogen chemistry, while also underscoring the limited availability of comparative data across oxidants under consistent experimental conditions.

In a companion study, we characterized the chemical composition and yield of laboratory SOA generated from the OH and Cl oxidation of *n*-dodecane and toluene, and the OH, Cl, and Br oxidation of isoprene and α-pinene.[125] While OH and Cl produced comparable SOA yields with oxygen-to-carbon (O/C) ratios indicative of multigenerational aging, Br-mediated SOA formation was more limited, yielding lower O/C values. These findings challenge model assumptions that Cl and Br produce SOA with similar efficiency.[127] To build on that work, this study characterizes the detailed molecular composition of gas- and condensed-phase products obtained from the reaction of α-pinene with OH, Cl, and Br in an oxidation flow reactor (OFR). Using an ammonium-adduct Vocus proton-transfer reaction time-of-flight mass spectrometer (PTR-ToF-MS) equipped with a vaporization inlet for aerosols (VIA), we detected a wide range of gas- and condensed-phase oxidation products. We applied PMF to classify these products and compared their composition and volatility across the three oxidants. These measurements provide new insight into the distinct pathways and product distributions associated with halogen- *versus* OH-mediated oxidation, with implications for the treatment of halogen chemistry in atmospheric models.

2 Experimental

2.1 Oxidation flow reactor setup

Experiments were conducted inside a Potential Aerosol Mass (PAM) OFR (Aerodyne Research), a 13 L horizontal aluminum cylindrical chamber (46 cm long × 22 cm ID) operated in continuous flow mode with a total flow of 6.0–6.8 L min^{-1}, yielding a calculated mean residence time (τ_{OFR}) of 114–130 s. An electroconductive Teflon coating was applied to the OFR to improve chemical compatibility with halogen precursors while maintaining high gas and particle transmission.[125,128] Two low-pressure mercury (Hg) lamps housed in type 214 quartz sleeves were used to photolyze oxidant precursors, with UV output regulated by a fluorescent dimming ballast (IZT-2S28-D, Advance Transformer Co.). The UV irradiance was controlled by adjusting the ballast control voltage (1.5–10 VDC) and measured using a TOCON-GaP6 photodetector (sglux GmbH). The corresponding actinic flux ranged from approximately 1 × 10^{14} to 3 × 10^{15} photons cm^{-2} s^{-1}.[129,130]

2.2 Oxidant, OVOC and SOA generation

OH was generated by photolyzing O_2 and H_2O at $\lambda = 185$ nm and O_3 at $\lambda = 254$ nm using two low-pressure Hg lamps. The relative humidity (RH) was controlled to 31–43% using a Nafion humidifier (Perma Pure); corresponding H_2O mixing ratios were 1.0–1.5% at OFR temperatures of 26–29 °C. The integrated OH

exposure (OH_{exp}) in the OFR, defined as the product of the mean OH concentration and τ_{OFR}, was calculated using an empirical estimation equation[130] and ranged from 6.7×10^{10} to 1.0×10^{12} molecules cm^{-3} s (hereafter "cm^{-3} s") – equivalent to 0.5–8 days of atmospheric oxidation at OH = 1.5×10^6 cm^{-3}.[131] The estimated uncertainty in calculated OH_{exp} values was ±50%. Cl was produced by photolyzing 4.2 ppm oxalyl chloride ($C_2Cl_2O_2$) at λ = 254 or 313 nm,[125,132,133] and Br was generated by photolyzing 1.8 ppm oxalyl bromide ($C_2Br_2O_2$) at λ = 254 nm.[125,134,135] These $C_2Cl_2O_2$ and $C_2Br_2O_2$ mixing ratios were chosen to ensure >99.5% consumption of α-pinene by reaction with Cl or Br at maximum actinic flux in the OFR. The RH in Cl and Br experiments was maintained at 1.1–4.1%; corresponding H_2O mixing ratios were 0.04–0.12% at OFR temperatures between 24–28 °C. Integrated Cl and Br exposures (Cl_{exp}, Br_{exp}) were characterized *via* offline calibration using O_3 decay measurements, with estimated uncertainties of ±70%.[125] Estimated Cl_{exp} values ranged from 4.6×10^8 to 1.3×10^{11} cm^{-3} s, and Br_{exp} values ranged from 4.5×10^{11} to 3.7×10^{12} cm^{-3} s, corresponding to 2 h – 25 days ([Cl] = 6×10^4 cm^{-3}) and 0.7–6 days ([Br] = 7×10^6 cm^{-3}) of equivalent atmospheric exposure.[136] Gas-phase OH, Cl, or Br oxidation of α-pinene led to the formation of OVOCs and SOA *via* homogeneous nucleation. α-Pinene (10% (v/v) in carbon tetrachloride) was injected into the OFR carrier gas flow at 0.94–2.8 μL h^{-1} using a syringe pump, yielding ~30 ppbv for OH and Cl experiments and ~90 ppbv for Br experiments to ensure nucleation.[125]

2.2.1 Caution. This study involved preparing polyfluorotetraethylene (PTFE) permeation tubes filled with liquid $C_2Cl_2O_2$ and $C_2Br_2O_2$,[125] which are toxic, corrosive, and release harmful gases upon decomposition. $C_2Cl_2O_2$ and $C_2Br_2O_2$ permeation tubes were prepared in a well-ventilated fume hood with appropriate personal protective equipment, including gloves, lab coats, and eye protection. O_3 is a strong oxidant and respiratory irritant. Exhaust flows containing O_3, $C_2Cl_2O_2$ or $C_2Br_2O_2$ were vented to a laboratory fume exhaust system to prevent exposure and accumulation.

2.3 Instrumentation

Aerosol number concentrations and size distributions were measured using a scanning mobility particle sizer (SMPS; TSI), and aerosol mass spectra were acquired using an Aerodyne long high-resolution time-of-flight aerosol mass spectrometer (L-ToF-AMS). Gas- and condensed-phase organic compounds were measured with a Vocus 2R PTR-ToF-MS[137] (hereafter referred to as "Vocus") following low-pressure ammonium adduct (NH_4^+) ionization.[138,139] The system alternated between gas-phase and particle-phase sampling using a PTFE solenoid valve manifold (Fig. 2). During gas sampling, the Vocus sampled the OFR through an unheated 0.25 in. o.d. fluorinated ethylene propylene (FEP) line with a PTFE membrane filter to remove particles. For particle sampling, the Vocus sampled the OFR through a charcoal denuder that removed gas-phase organics before evaporation of aerosols in a heated (220 °C) Sulfinert-coated stainless-steel VIA[140–142] at a flow of 1.5 slpm.

2.4 Data analysis

L-ToF-AMS mass spectra were analyzed using SQUIRREL version 1.63I and PIKA version 1.23I[143] software, and elemental analysis of high-resolution L-ToF-AMS spectra was performed using the "Improved-Ambient" method.[143,144] High-resolution Vocus mass spectra were analyzed using Tofware version 3.2.5.[145] To aid in the interpretation of Vocus mass spectra,

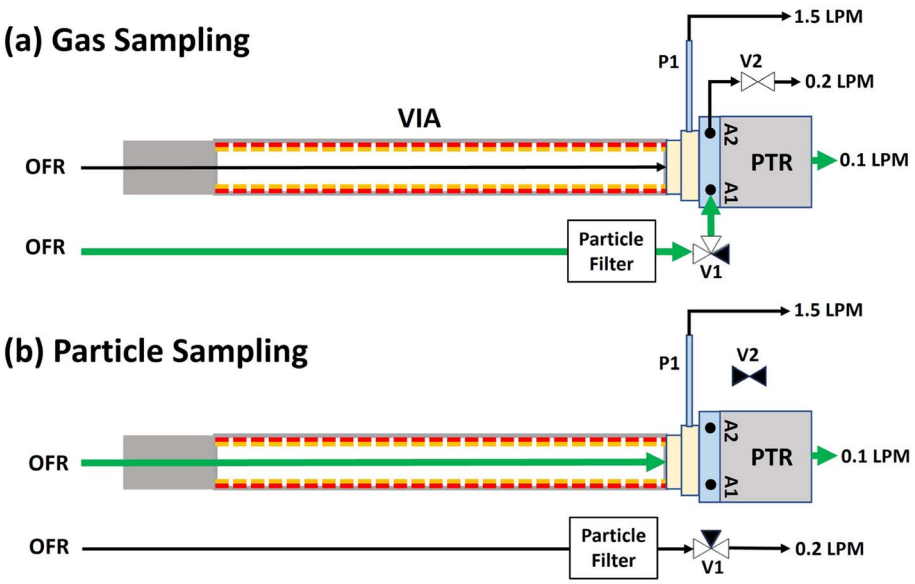

Fig. 2 Schematic of (a) gas and (b) particle sampling Vocus configurations used in these experiments. During gas sampling (a), the OFR was sampled through an unheated 0.25 in. o.d. FEP inlet line that was connected to Vocus atmospheric pressure ports A1 and A2. Aerosols were removed using a PTFE membrane filter upstream of three-way valve V1, and sample flow pulled through the VIA was removed through inlet pump port P1. During particle sampling (b), the OFR was sampled through an activated charcoal denuder and the VIA (T = 220 °C), while the unheated FEP inlet line was isolated from the Vocus by switching V1 and closing on/off valve V2. Constant flows were continuously pulled through P1 and either A1 and A2 or pumped to exhaust, while 0.1 L min^{-1} flow was continuously subsampled into the Vocus PTR reactor.

PMF[146] was applied to NH_4^+ adduct signals with even m/z values between $m/z = 150$ and 350, exported from Tofware. This range and selection minimized interference from low-mass background and fragment ions in the mass spectra. Ion-specific errors were calculated as $1.28\sqrt{I}$,[147] where I is the high-resolution peak height. PMF was used primarily to group ions with similar temporal behavior trends and to qualitatively apportion ions contributing to multiple factors. Separate PMF analyses were performed for the α-pinene/OH, α-pinene/Cl, and α-pinene/Br systems using the PMF Evaluation Tool (PET) version 3.08C,[148] each yielding a four-factor solution representing precursors and early- and late-generation products. Three-factor PMF tended to combine precursor and product signals, often with higher residuals. Solutions with five or more factors led to the splitting of existing factors without identifying new product groups of products or significantly reducing residuals. To avoid artificially forcing ion signals to zero in specific factors, no rotations were applied.

2.5 Effective saturation concentration (C°) calculations

C° values for $C_{10}H_{14,16}O_x$ compounds were calculated using the empirical formula: $\log(C^\circ) = 0.475(25 - n_C) - 2.3n_O + 0.6\frac{n_C n_O}{n_C + n_O}$,[149] where n_C and n_O are the carbon and oxygen numbers of each compound. Vocus:VIA-Vocus ratios of measured $C_{10}H_{14,16}O_x$ compounds were plotted against their calculated C° values and fit to sigmoid or polynomial regression equations. These equations were then used to infer C° for $C_{10}H_{13,15}ClO_x$ and $C_{10}H_{13,15}BrO_x$ from their measured Vocus:VIA-Vocus ratios. This analysis was restricted to $C_{10}H_{14,16}O_x$, $C_{10}H_{13,15}ClO_x$ and $C_{10}H_{13,15}BrO_x$ signals to minimize the effect of possible thermal decomposition reactions in the VIA on the calculated C° values.

2.6 Peroxy radical fate modeling

To explore the fate of RO_2 generated from OH, Cl, and Br oxidation of α-pinene, we used the KinSim chemical kinetic solver[150] with a simplified mechanism adapted from prior OFR studies.[125,130,151,152] In the model, RO_2 were generated from the reactions

$$\text{APINENE} + \text{OH} \rightarrow \text{RO}_2$$

$$\text{APINENE} + \text{Cl} \rightarrow \text{RO}_2$$

$$\text{APINENE} + \text{Br} \rightarrow \text{RO}_2$$

While RO_2 composition varies across the OH, Cl, and Br systems, we assumed that rate coefficients for RO_2 remained the same due to the lack of kinetic data. Following the approach introduced by Peng *et al.*[153] and used in previous studies by our group[141,154] we applied kinetic data and reaction pathways associated with reactions between Cl/Br and the methylperoxy radical (CH_3O_2) as a surrogate RO_2 species. These RO_2 were assumed to undergo autooxidation *via* isomerization, react with other RO_2, and/or react with hydroperoxyl radicals (HO_2):

$$\text{RO}_2 + \text{O}_2 \rightarrow \text{RO}_{2,\text{isom}}$$

$$\text{RO}_2 + \text{RO}_2 \rightarrow 2\text{RO} + \text{O}_2$$

$$\text{RO}_2 + \text{RO}_2 \rightarrow \text{ROH} + \text{R(O)} + \text{O}_2$$

$$\text{RO}_2 + \text{RO}_{2,\text{isom}} \rightarrow 2\text{RO} + \text{O}_2$$

$$\text{RO}_2 + \text{RO}_{2,\text{isom}} \rightarrow \text{ROH} + \text{R(O)} + \text{O}_2$$

$$\text{RO}_2 + \text{HO}_2 \rightarrow \text{ROOH}$$

$$\text{RO}_{2,\text{isom}} + \text{HO}_2 \rightarrow \text{ROOH}$$

Here, RO, ROH, R(O), and ROOH denote generic alkoxy radical, alcohol, carbonyl, and organic peroxide species, respectively. In the α-pinene/OH system, we assumed RO_2 reacted with OH to generate ROH and O_2,[155] and that RO isomerized and decomposed to generate pinonaldehyde (PINAL) and HO_2:[156]

$$\text{RO}_2 + \text{OH} \rightarrow \text{ROH} + \text{O}_2$$

$$\text{RO}_{2,\text{isom}} + \text{OH} \rightarrow \text{ROH} + \text{O}_2$$

$$\text{RO} + \text{O}_2 \rightarrow \text{PINAL} + \text{HO}_2$$

In the α-pinene/Cl system, we assumed RO_2 reacted with Cl to generate RO and ClO,[44] and that RO_2 reacted with ClO to generate RO and ClO_2 or organic chlorides (ROCl) and O_2.[59] We also assumed that all RO generated from $RO_2 + RO_2$ and RO_2 + Cl reactions were chlorinated, and that they subsequently isomerized and decomposed to yield either chloropinonaldehyde (CHLOROPINAL) and HO_2, or pinonaldehyde and Cl,[122] with branching ratios of 0.33 and 0.67 respectively:[126]

$$\text{RO}_2 + \text{Cl} \rightarrow \text{RO} + \text{ClO}$$

$$\text{RO}_{2,\text{isom}} + \text{Cl} \rightarrow \text{RO} + \text{ClO}$$

$$\text{RO}_2 + \text{ClO} \rightarrow \text{RO} + \text{ClO}_2$$

$$\text{RO}_{2,\text{isom}} + \text{ClO} \rightarrow \text{RO} + \text{ClO}_2$$

$$\text{RO}_2 + \text{ClO} \rightarrow \text{ROCl} + \text{O}_2$$

$$\text{RO}_{2,\text{isom}} + \text{ClO} \rightarrow \text{ROCl} + \text{O}_2$$

$$\text{RO} + \text{O}_2 \rightarrow \text{CHLOROPINAL} + \text{HO}_2$$

$$\text{RO} + \text{O}_2 \rightarrow \text{PINAL} + \text{Cl}$$

In the α-pinene/Br system, we assumed RO_2 reacted with Br to generate RO and BrO,[157] and that RO_2 reacted with BrO to generate RO_2H and HOBr.[158,159] We also assumed all RO generated from $RO_2 + RO_2$ and RO_2 + Br were brominated, and that they isomerized and decomposed to produce either bromopinonaldehyde (BROMOPINAL) and HO_2, or pinonaldehyde and Br, with branching ratios of 0.66 and 0.34 respectively:[126]

$$RO_2 + Br \rightarrow RO + BrO$$

$$RO_{2,isom} + Br \rightarrow RO_2$$

$$RO_2 + BrO \rightarrow RO_2H + HOBr$$

$$RO_{2,isom} + BrO \rightarrow RO_2H + HOBr$$

$$RO + O_2 \rightarrow BROMOPINAL + HO_2$$

$$RO + O_2 \rightarrow PINAL + Br$$

Finally, RO_2 were regenerated following reaction of ROH, R(O), ROOH, RO_2H, ROCl, PINAL, CHLOROPINAL, and BROMOPINAL with OH, Cl, and Br:

$$ROH + OH/Cl/Br \rightarrow RO_2$$

$$R(O) + OH/Cl/Br \rightarrow RO_2$$

$$ROOH + OH/Cl/Br \rightarrow RO_2$$

$$ROCl + Cl \rightarrow RO_2$$

$$PINAL + OH/Cl/Br \rightarrow RO_2$$

$$CHLOROPINAL + Cl \rightarrow RO_2$$

$$BROMOPINAL + Br \rightarrow RO_2$$

$$RO_2H + Br \rightarrow RO_2$$

The kinetic parameters used in these calculations[16,19,37,44,50,53,59,79,107,156,158,160–165] are listed in Table S2, with the following additional assumptions:

1. A bimolecular rate coefficient of 1.6×10^{-10} cm^3 s^{-1} for $RO_2 + Br \rightarrow RO + BrO$.

2. Rate coefficients for ROH + Cl, R(O) + Cl, and ROOH + Cl reactions were 10 times faster than the corresponding ROH + OH, R(O) + OH, and ROOH + OH rate coefficients.

3. Rate coefficients for ROH + Br, R(O) + Br, and ROOH + Br reactions were 100 times slower than the α-pinene + Br rate coefficient.

4. Secondary OH production from halogen-initiated α-pinene oxidation was negligible.

Simulations were run with and without isomerization pathways, assuming first-order isomerization rate coefficients of 0, 0.1, 1, and 4 s^{-1}.[163,165] Results from these simulations were used to calculate the fractional loss of generic RO_2 (denoted F_{RO_2}) as a function of OH_{exp}, Cl_{exp}, and Br_{exp}.

3 Results & discussion

3.1 Overview of results obtained from alternating Vocus and VIA-Vocus measurements

Fig. S1 shows example time series of Vocus signals collected during an α-pinene/Cl experiment, alternating between Vocus and VIA-Vocus sampling modes every 15 min. Fig. S1a displays Cl_{exp}, which was varied in discrete steps from 0 to 1.2×10^{11} cm^{-3} s throughout the experiment, and Fig. S1b–e show representative ammonium adduct ion signals exhibiting distinct trends with Cl_{exp}. In Fig. S1b, the signal for unreacted α-pinene ($NH_4^+ \cdot C_{10}H_{16}$) was highest at low Cl_{exp} and decreased with increasing Cl_{exp}, as expected. At low Cl_{exp}, $NH_4^+ \cdot C_{10}H_{16}$ signal was enhanced during Vocus sampling periods but was negligible during VIA-Vocus sampling periods due to its removal by the charcoal denuder upstream of the VIA. Fig. S1c shows that $NH_4^+ \cdot C_{10}H_{15}ClO_2$ also peaked during Vocus sampling and reached maximum intensity at intermediate Cl_{exp}, suggesting it is an early-generation gas-phase oxidation product. Its decline at higher Cl_{exp} likely reflects further oxidation to more functionalized compounds. In Fig. S1d, both $NH_4^+ \cdot C_3H_6O$ and its chlorinated analog $NH_4^+ \cdot C_3H_5ClO$ plateau at intermediate-to-high Cl_{exp}, consistent with their formation as fragmentation products from α-pinene and/or its early-generation oxidation products. Finally, Fig. S1e shows $NH_4^+ \cdot C_{10}H_{14}O_7$ and $NH_4^+ \cdot C_{10}H_{13}ClO_7$, which peaked at higher Cl_{exp} and were enriched during VIA-Vocus sampling, indicating their

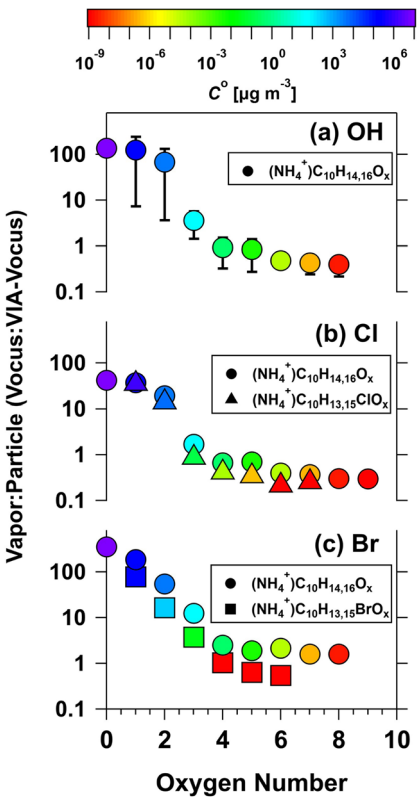

Fig. 3 Ratio of Vocus to VIA-Vocus signal intensities (Vocus : VIA) for C_{10} ammonium adducts as a function of oxygen number, measured during α-pinene oxidation experiments with (a) OH, (b) Cl, and (c) Br as the primary oxidants. Circle symbols represent non-halogenated species ($NH_4^+ \cdot C_{10}H_{14,16}O_x$), triangles represent chlorinated species ($NH_4^+ \cdot C_{10}H_{13,15}ClO_x$), and squares represent brominated species ($NH_4^+ \cdot C_{10}H_{13,15}BrO_x$). Colors indicate estimated volatility (C^*) from 10^{-9} to 10^7 μg m^{-3}. C^* values were calculated using methods described in Section 2.5.

low volatility and likely contribution to SOA. Similar trends were observed in α-pinene/OH and α-pinene/Br experiments. Additional compounds with analogous temporal behavior were identified with PMF and are discussed in the next section.

To examine how Vocus : VIA-Vocus signal ratios relate to compound volatility, Fig. 3 presents three panels showing the ratio of Vocus to VIA-Vocus signals for C_{10} species detected in α-pinene/OH, α-pinene/Cl, and α-pinene/Br experiments, plotted as a function of oxygen number. Symbols are colored by $C°$, ranging from approximately 10^7 μg m^{-3} (purple) to 10^{-8} μg m^{-3} (red). In Fig. 3a, α-pinene/OH products show a clear trend: as oxygen number (n_O) increases from 0 to 8, the Vocus : VIA-Vocus ratio decreases from approximately 137 to 0.4, $C°$ decreases. Compounds with $n_O \approx$ 0–2 exhibit high $C°$ values (10^4–10^7 μg m^{-3}), consistent with dominant gas-phase behavior, and compounds with n_O = 3–5 and $C° \approx$ 0.1–10 μg m^{-3} show comparable signals in both configurations, consistent with semivolatile behavior. Highly oxygenated species ($n_O \geq 6$) exhibit $C° < 10^{-3}$ μg m^{-3} and low Vocus : VIA-Vocus ratios, indicating low volatility and likely contribution to SOA.

Fig. 3b compares Vocus : VIA-Vocus ratios for non-halogenated (circles) and chlorinated (triangles) species from α-pinene/Cl experiments. Both groups show decreasing Vocus : VIA-Vocus ratios and $C°$ with higher n_O. Chlorinated compounds generally have similar or slightly lower $C°$ than their non-halogenated counterparts. Cl-containing species with n_O = 1–2 behave predominantly as gases, n_O = 3 are semivolatile, and $n_O \geq 4$ mostly partition to the condensed phase. Fig. 3c shows analogous results for brominated products (squares), alongside non-halogenated compounds (circles) from α-pinene/Br experiments. Similar trends are observed: Vocus : VIA-Vocus ratios and $C°$ values decrease with n_O. Br-containing compounds with n_O = 1–2 are mainly in the gas phase, n_O = 3 are semivolatile, and $n_O \geq 4$ are low-volatility and likely mostly in the condensed-phase. Overall, Fig. 3 demonstrates a strong correlation between n_O and volatility. Higher n_O corresponds to lower Vocus : VIA-Vocus ratios and $C°$ values, indicating enhanced partitioning to the condensed phase. The presence of Cl or Br further modulates this trend, generally lowering volatility and increasing the likelihood of SOA formation relative to non-halogen species with equal n_O. To extend the volatility estimation framework of Donahue *et al.*,[149] which relates log($C°$) to molecular composition for CHO compounds, we adapted the formulation to include chlorinated (CHOBr) and brominated (CHOBr) species. The modified expression is:

$$\log(C°) = 0.475(25 - n_C) - 2.3n_O + 0.6\frac{n_C n_O}{n_C + n_O} - b_{Cl}n_{Cl} - b_{Br}n_{Br} \quad (1)$$

where n_{Cl} and n_{Br} are the numbers of Cl and Br atoms, and b_{Cl} and b_{Br} represent their respective contributions to log($C°$). For compounds with $n_O \geq$3, Fig. 3b and c suggest that Cl and Br decrease volatility comparably to the addition of ~2 and ~4 oxygen atoms, respectively; that is, $b_{Cl} \approx 2b_O$ and $b_{Br} \approx 4b_O$. Assuming $b_O \approx$ 2.3,[149] we arrive at the following revised formulation:

$$\log(C°) = 0.475(25 - n_C) - 2.3n_O + 0.6\frac{n_C n_O}{n_C + n_O} - 4.6n_{Cl} - 9.2n_{Br} \quad (2)$$

While beyond the scope of this work, a more comprehensive characterization of b_{Cl} and b_{Br} using the approach of Li *et al.*[166] should be explored in future studies.

3.2 Molecular characterization of α-pinene/OH, α-pinene/Cl, and α-pinene/Br oxidation products

3.2.1 α-Pinene/OH. Fig. 4 presents results from PMF analysis of α-pinene/OH oxidation products detected with the Vocus. Four factors were identified, each characterized by its evolution with OH_{exp} (Fig. 4a, c, e and g) and corresponding Kendrick Mass Defect (KMD) plots (Fig. 4b, d, f and h), where symbol size is proportional to signal intensity. Factor 1 ("VOC/OVOC1") consists primarily of gas-phase species detected in Vocus mode (Fig. 4a). Its signal peaks at the lowest OH_{exp} and decreases rapidly, approaching zero by approximately 4×10^{11} cm^{-3} s. The dominant signals include α-pinene ($NH_4^+ \cdot C_{10}H_{16}$), $NH_4^+ \cdot C_{10}H_{14}O$ and $NH_4^+ \cdot C_{10}H_{16}O$ (Fig. 4b). These signals likely represent unreacted precursor and either α-pinene impurities that the Vocus is highly sensitive to, or early-generation oxidation products that PMF could not fully separate from α-pinene due to their fast formation and consumption. Factor 2 ("OVOC2") also comprises gas-phase compounds, peaking at $OH_{exp} \approx 1 \times 10^{11}$ cm^{-3} s before decreasing (Fig. 4c.). Major signals include $NH_4^+ \cdot C_{10}H_{16}O_2$ – possibly contributed from pinonaldhyde, 2-hydroxy-3-pinanone, and/or α-pinene hydroperoxide[156,167] – and $NH_4^+ \cdot C_9H_{14}O_4$, likely representing pinic acid[167] (Fig. 4d). Other species include $NH_4^+ \cdot C_{10}H_{14}O_2$, $NH_4^+ \cdot C_{10}H_{16}O$, and various C_8–C_{10} compounds. Factor 3 ("OVOC3") peaks at $OH_{exp} \approx 4 \times 10^{11}$ cm^{-3} s and then gradually declines (Fig. 4e). Like the previous factors, it primarily consists of gas-phase species. Although $NH_4^+ \cdot C_3H_6O$ was excluded from the PMF analysis because it was below m/z 150 (Sect. 2.4), its temporal trend matches this factor. Major constituents include $NH_4^+ \cdot C_5H_8O_4$ and $NH_4^+ \cdot C_5H_8O_5$, with additional contributions from $NH_4^+ \cdot C_4H_6O_{5-6}$, $NH_4^+ \cdot C_{6,7}H_8O_{4-7}$, $NH_4^+ \cdot C_7H_{10}O_{4-6}$, and $NH_4^+ \cdot C_8H_{12}O_{2-4}$ (Fig. 4f). These species generally have lower n_C and higher n_O than those in Factors 1 and 2. Factor 4 ("SOA") includes 70 signals dominated by low-volatility, condensed-phase compounds and peaks at $OH_{exp} = 2.3 \times 10^{11}$ cm^{-3} s (Fig. 4g), suggesting formation *via* continued oxidation of Factor 2 compounds. The KMD plot shows a complex mixture of highly oxygenated C_4 to C_{10} compounds (Fig. 4h).

The Factor 4 elemental composition is further examined in Fig. 5, which overlays the H/C and O/C ratios of individual factor compounds on a Van Krevelen diagram, allowing qualitative assessment of their contributions to ensemble O/C and H/C ratios derived from L-ToF-AMS measurements of α-pinene OH-SOA. Several prominent homologous series of C_5–C_{10} compounds are evident. To contextualize observed oxidation products in terms of known α-pinene/OH chemistry, we compared measured molecular formulas to those predicted by the Master Chemical Mechanism (MCM), a near-explicit gas-

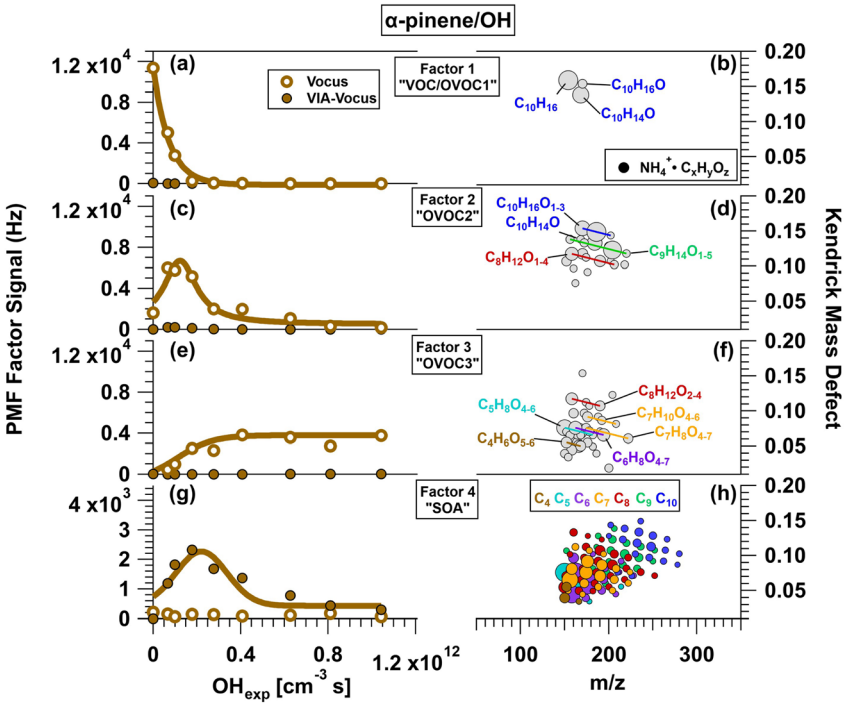

Fig. 4 Results from PMF analysis of Vocus and VIA-Vocus measurements of the α-pinene + OH system. (a, c, e and g) Signals of four distinct factors as a function of OH exposure (OH_{exp}): initial α-pinene precursor (Factor 1), gas-phase oxidation products (Factors 2 and 3), and condensed-phase oxidation products (Factor 4). (b, d, f and h) Corresponding Kendrick Mass Defect (KMD) plots showing the chemical composition of each factor. Symbol size is proportional to signal intensity. For clarity, only species with relative abundances ≥ 0.040 (Factor 1), 0.0080 (Factor 2), 0.0044 (Factor 3), and 0.002 (Factor 4) are shown.

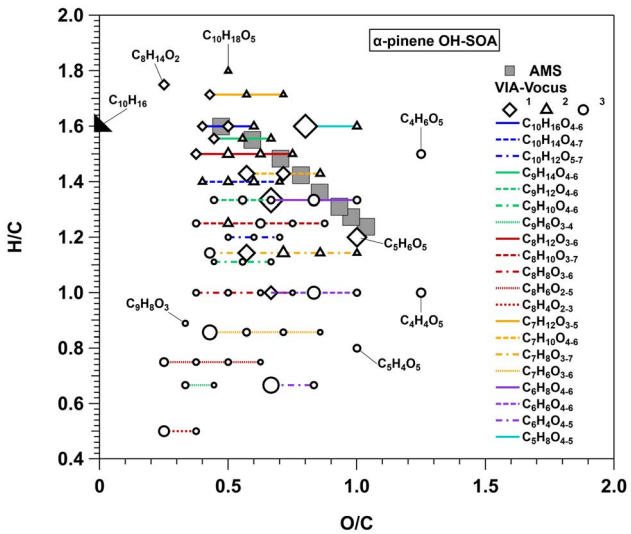

Fig. 5 Van Krevelen diagram showing H/C and O/C ratios of SOA generated from the OH oxidation of α-pinene. L-ToF-AMS data (gray squares) show bulk SOA elemental composition, while VIA-Vocus data (diamonds/triangles/circles) identify individual molecular formulas of Factor 4 components (Fig. 4). Colored lines show homologous series of oxidation products. Additional figure notes: [1]molecular formulas of oxidation products included in the Master Chemical Mechanism (MCM);[156] [2]molecular formulas of previously-reported oxidation products that are not included in the MCM,[168–174] [3]molecular formulas not previously reported in α-pinene/OH studies.

phase chemical model that describes the degradation of VOCs like α-pinene through detailed reaction pathways.[156] Here, diamond symbols denote molecular formulas represented in the MCM, including the largest signal, $NH_4^+ \cdot C_5H_8O_4$, which may originate from 3-hydroperoxy-4-oxo-pentanal ("C511OOH" in the MCM) and/or 3-hydroxy-4-oxopentanoic acid ("H3C2C4CO2H"). Similarly, $NH_4^+ \cdot C_6H_8O_4$ may arise from 6-hydroxyhexane-2,3,5-trione ("C614CO") and/or 4-hydroxy-2,5-dioxi-hexanal ("H3C25C5CHO"). Structures and formulas for MCM-predicted and detected compounds are shown in Fig. S2. Triangle symbols represent known α-pinene products that are not included in the MCM, such as terpenylic and 2-hydroxyterpenylic acids ($NH_4^+ \cdot C_8H_{12}O_{4-5}$), diaterpenylic acid acetate ($NH_4^+ \cdot C_{10}H_{16}O_6$),[168] and 3-methyl-1,2,3-butanetricarboxylic acid ($NH_4^+ \cdot C_8H_{12}O_6$),[169,170] along with others.[171–174] Circle symbols denote 39 molecular formulas not previously reported in α-pinene/OH oxidation studies. Some may result from thermal degradation in the VIA, especially those with low H/C ratios ($0.5 \leq H/C < 1$). Others may represent later-generation oxidation products formed *via* functionalization or fragmentation of known precursors. For example, $NH_4^+ \cdot C_6H_{6,8}O_{5-6}$ may result from alcohol addition to $C_6H_{6,8}O_4$-type compounds like "CO235C5CHO", "C614CO" and/or "H3C25C5CHO", while $NH_4^+ \cdot C_{10}H_{12}O_{5-7}$ may result from addition of two carbonyl groups to known $C_{10}H_{16}O_{3-5}$ products,[171] along with other possible pathways. Additional signals such as $NH_4^+ \cdot C_4H_{4,6}O_5$

likely stem from OH-initiated fragmentation of earlier-generation α-pinene/OH oxidation products.

3.2.2 α-Pinene/Cl. Fig. 6 presents the PMF analysis of α-pinene/Cl oxidation products measured with the Vocus. As with the α-pinene/OH system, four distinct factors were identified, each characterized by unique mass spectral signatures and trends with Cl_{exp}. Factor 1 closely resembles Factor 1 from the α-pinene/OH system. It consists mainly of unreacted α-pinene plus $NH_4^+ \cdot C_{10}H_{14}O$ and $NH_4^+ \cdot C_{10}H_{16}O$, and its signal decreases steadily with increasing Cl_{exp}. Factor 2 contains gas-phase species and peaks at $Cl_{exp} \approx 5.3 \times 10^{10}$ cm^{-3} (Fig. 6c). The largest contributor is $NH_4^+ \cdot C_{10}H_{14}O$, followed by chlorinated compounds including $NH_4^+ \cdot C_{10}H_{15}ClO$, $NH_4^+ \cdot C_{10}H_{17}ClO$, and $NH_4^+ \cdot C_{10}H_{15}ClO_2$, along with additional chlorinated and non-chlorinated adducts. Factor 3 also contains gas-phase compounds, but its signal increases continuously with Cl_{exp}. It includes $NH_4^+ \cdot C_5H_6Cl_2O_2$, $NH_4^+ \cdot C_6H_9ClO_2$, and $NH_4^+ \cdot C_7H_9ClO_3$, along with 33 other C_3–C_9 chlorinated and non-chlorinated species. $NH_4^+ \cdot C_3H_6O$ and its $NH_4^+ \cdot C_3H_5ClO$ chlorinated analog followed a similar trend, but plateaued at lower Cl_{exp} than Factor 3; additionally, the yield of $NH_4^+ \cdot C_3H_6O$ was lower than in the α-pinene/OH system. Factor 4 is composed primarily of low-volatility, condensed-phase products and peaks at $Cl_{exp} \approx 8.2 \times 10^{10}$ cm^{-3} s (Fig. 6g), suggesting it results from continued oxidation of compounds in Factor 2. Like the α-pinene OH-SOA factor, this Cl-SOA factor is chemically complex, containing 45 chlorinated and 87 non-chlorinated C_4 to C_{10} ammonium adducts.

Factor 4 components are examined in detail in Fig. S3a and b, which plot their H/C and O/C ratios on Van Krevelen diagrams, alongside ensemble AMS-derived O/C and H/C ratios for α-pinene Cl-SOA. Given the greater complexity of α-pinene Cl-SOA compared to α-pinene OH-SOA, formulas for non-chlorinated ($NH_4^+ \cdot C_xH_yO_z$) and chlorinated ($NH_4^+ \cdot C_xH_yCl_wO_z$) compounds are shown separately. Triangle symbols represent species previously reported by Masoud and Hildebrandt Ruiz,[124] including 37 of the 87 non-chlorinated compounds and 10 of the 45 chlorinated compounds. The only other study characterizing α-pinene/Cl oxidation products used a method selective for highly oxygenated organic molecules (HOM)[123] which NH_4^+ CIMS is less sensitive to. Circle symbols represent compounds not previously reported in α-pinene/Cl oxidation studies. As with the α-pinene/OH system, species with low H/C ratios ($0.5 \leq H/C < 1$) may result from thermal decomposition in the VIA. Non-chlorinated species detected in Cl-SOA include many also observed in α-pinene OH-SOA, though with different relative abundances. The most intense were $NH_4^+ \cdot C_7H_8O_4$ and $NH_4^+ \cdot C_6H_8O_4$. Species present in OH-SOA but largely absent in Cl-SOA include: $C_4H_6O_5$, $C_7H_{12}O_5$, $C_8H_{10}O_{6-7}$, $C_8H_{12}O_6$, $C_8H_{14}O_2$, $C_{10}H_{16}O_{5-6}$, and $C_{10}H_{18}O_5$. Conversely, non-chlorinated species enriched in Cl-SOA include $C_8H_{10,12}O_2$, $C_9H_{10}O_{1-3}$, $C_9H_{12,14}O_{2-3}$, $C_{10}H_{12}O_{2-4}$, and $C_{10}H_{14}O_{1-3}$. These are likely thermal or fragmentation artifacts, given their volatilty and absence in OH-SOA. Some may also result from HCl eliminations not present in the α-pinene/OH system. Chlorinated adducts in the Cl-SOA include $NH_4^+ \cdot C_6H_7ClO_3$ (most abundant), $NH_4^+ \cdot C_5H_7ClO_{2-3}$,

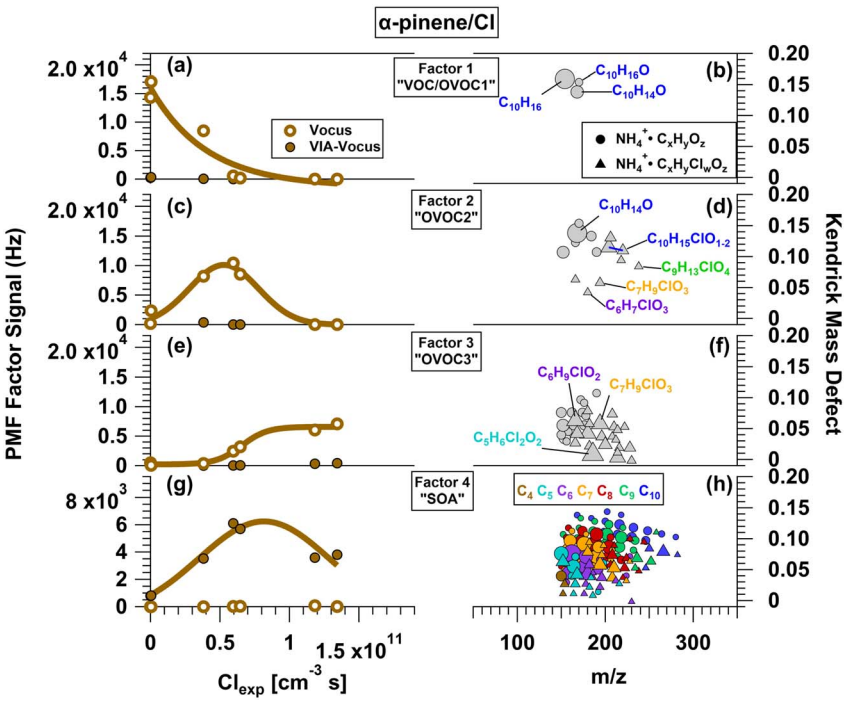

Fig. 6 Results from PMF analysis of Vocus and VIA-Vocus measurements of the α-pinene + Cl system. (a, c, e and g) Signals of four distinct factors as a function of Cl exposure (Cl_{exp}): initial α-pinene precursor (Factor 1), gas-phase oxidation products (Factors 2 and 3), and condensed-phase oxidation products (Factor 4). (b, d, f and h) Corresponding KMD plots showing the chemical composition of each factor. Symbol size is proportional to signal intensity. For clarity, only species with relative abundances ≥ 0.043 (Factor 1), 0.010 (Factor 2), 0.0059 (Factor 3), and 0.0015 (Factor 4) are shown.

$NH_4^+ \cdot C_7H_9ClO_{3-4}$, and $NH_4^+ \cdot C_{10}H_{13}ClO_5$. In α-pinene OH-SOA, $NH_4^+ \cdot C_6H_8O_4$ was hypothesized to originate from "C614CO" and/or "H3C25C5CHO" based on MCM predictions. The presence of the corresponding chlorinated analog $NH_4^+ \cdot C_6H_7ClO_3$ suggests Cl-initiated oxidation of similar precursors. Analogous relationships likely exist between $NH_4^+ \cdot C_5H_8O_4$ and $NH_4^+ \cdot C_5H_7ClO_3$, and between $NH_4^+ \cdot C_7H_{10}O_{4-5}$ and $NH_4^+ \cdot C_7H_9ClO_{3-4}$.

3.2.3 α-Pinene/Br. Fig. 7 presents the PMF analysis of α-pinene/Br oxidation products measured with the Vocus. Factor 1 closely resembles the first factor in the OH and Cl systems – it is dominated by unreacted α-pinene, $NH_4^+ \cdot C_{10}H_{14}O$, and $NH_4^+ \cdot C_{10}H_{16}O$, and its signal decreases steadily with Br_{exp}. Factor 2 contains gas-phase species, peaking at $Br_{exp} \approx 2 \times 10^{12}$ cm^{-3} s before decreasing (Fig. 7c). The largest signal is $NH_4^+ \cdot C_{10}H_{14}O$, followed by $NH_4^+ \cdot C_9H_{10}O$, $NH_4^+ \cdot C_{10}H_{13}BrO$, $NH_4^+ \cdot C_{10}H_{14,16}O_2$, and $NH_4^+ \cdot C_{10}H_{15}BrO_{1,2}$. Factor 3 includes predominantly C_3–C_6 brominated gas-phase species whose signals increase with Br_{exp}, suggesting progressive fragmentation or oxidation of larger molecules. The dominant signal is $NH_4^+ \cdot C_3H_5BrO$, along with lesser signals from $NH_4^+ \cdot C_9H_{10}O$ and C_4–C_6 species such as $NH_4^+ \cdot C_4H_{5,7}BrO_2$, $NH_4^+ \cdot C_5H_{5,7}BrO_2$, $NH_4^+ \cdot C_5H_7BrO_3$, and $NH_4^+ \cdot C_6H_{7,9}BrO_2$. $NH_4^+ \cdot C_3H_6O$ plateaued at lower Br_{exp} than Factor 3 and at lower yield than in the α-pinene/OH system, similar to its behavior in the α-pinene/Cl system.

Factor 4 represents condensed-phase products and peaks at $Br_{exp} \approx 2.4 \times 10^{12}$ cm^{-3} s (Fig. 7g), suggesting formation *via* further oxidation of Factor 2 species. This factor includes 57 brominated and 77 non-brominated C_3 to C_{10} ammonium adducts. Their H/C and O/C ratios are shown in Van Krevelen space in Fig. S4a and b alongside α-pinene Br-SOA elemental ratios measured by L-ToF-AMS. As with Cl-SOA, brominated and non-brominated formulas are plotted separately. To our knowledge, this is the first study to report the molecular composition of α-pinene/Br oxidation products. As with the OH and Cl systems, species with $0.5 \leq H/C < 1$ are likely artifacts of thermal decomposition in the VIA. Many of the nonbrominated compounds shown in Fig. S4a overlap with those found in OH- and Cl-SOA, though in different proportions. The most abundant are $NH_4^+ \cdot C_{10}H_{14}O_4$, $NH_4^+ \cdot C_6H_{6,8}O_4$, and $NH_4^+ \cdot C_7H_8O_{3,4}$. Unique to the Br system are $NH_4^+ \cdot C_6H_{12}O_3$ and $NH_4^+ \cdot C_6H_{10}O_4$, which were not significant in OH-/Cl-SOA. Fig. S4b shows that the most intense brominated signal is $NH_4^+ \cdot C_3H_5BrO$ – likely bromoacetone – which is too volatile to be a true condensed-phase species. Its Vocus : VIA-Vocus ratio was nearly 100, qualitatively consistent with other volatile C_{10} species (Fig. 3) and suggesting possible charcoal denuder breakthrough from the gas phase. After $NH_4^+ \cdot C_3H_5BrO$, the next largest brominated adducts are $NH_4^+ \cdot C_{10}H_{13,15}BrO_{3,4}$. While the Br-SOA composition differs markedly from OH- and Cl-SOA, some chemical parallels remain. For instance, α-pinene/OH pathways in the

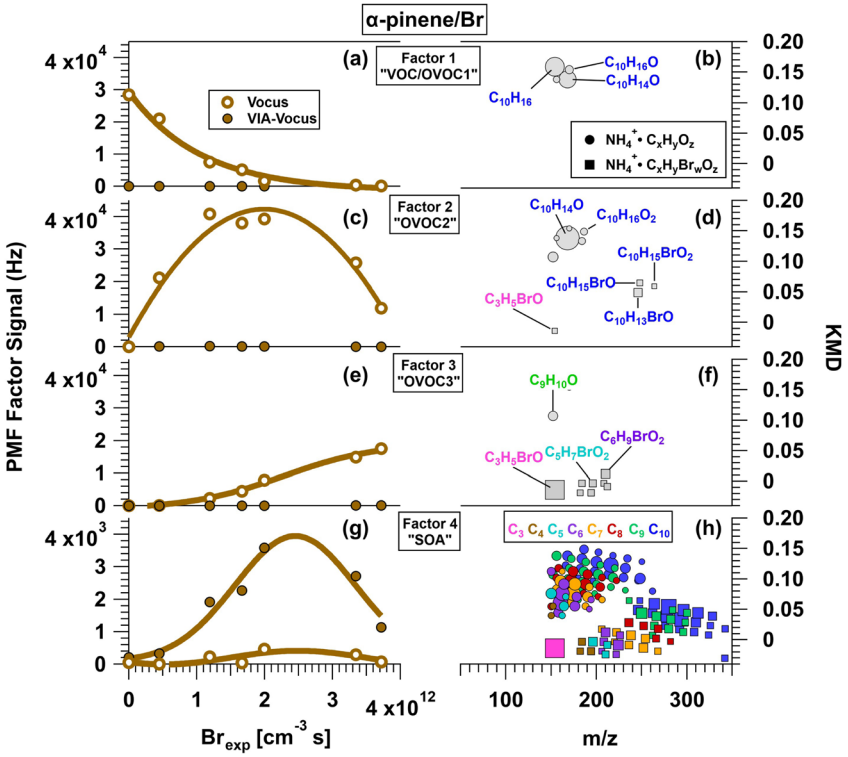

Fig. 7 Results from PMF analysis of Vocus and VIA-Vocus measurements of the α-pinene + Br system. (a, c, e and g) Signals of four distinct factors as a function of Br exposure (Br_{exp}): initial α-pinene precursor (Factor 1), gas-phase oxidation products (Factors 2 and 3), and condensed-phase oxidation products (Factor 4). (b, d, f and h) Corresponding KMD plots showing the chemical composition of each factor. Symbol size is proportional to signal intensity. For clarity, only species with relative abundances ≥0.031 (Factor 1), 0.014 (Factor 2), 0.012 (Factor 3), and 0.0026 (Factor 4) are shown.

MCM leading to"PINALOH" ($C_{10}H_{16}O_3$) and "C106OH" ($C_{10}H_{16}O_4$) can be adapted to α-pinene/Br chemistry. Br-initiated oxidation of bromopinonaldehyde ($C_{10}H_{15}BrO_2$) may produce a $C_{10}H_{14}BrO_4$ peroxy radical, followed by RO_2 + RO_2 forming a $C_{10}H_{14}BrO_3$ alkoxy radical and subsequent $C_{10}H_{13}BrO_3$ (carbonyl) and $C_{10}H_{15}BrO_3$ (alcohol) products. Further isomerization and O_2 addition yield a $C_{10}H_{15}BrO_5$ peroxy radical, which could react with RO_2 again to produce $C_{10}H_{13,15}BrO_4$ carbonyl and alcohol products.

3.3 Comparison of α-pinene/OH, α-pinene/Cl, and α-pinene/Br OVOC and SOA factors

Comparison of Fig. 4d, 6d and 7d reveals notable differences in the composition of the "OVOC2" factors derived from α-pinene oxidation by OH, Cl and Br. In the Cl and Br systems, we hypothesize that $NH_4^+ \cdot C_{10}H_{15}ClO$, $NH_4^+ \cdot C_{10}H_{17}ClO$ and $NH_4^+ \cdot C_{10}H_{15}BrO$ are first-generation products formed *via* halogen addition to the α-pinene endocyclic double bond, followed by RO_2 + RO_2 reactions. This is analogous to OH-initiated oxidation in the MCM, which generates $C_{10}H_{16}O_2$ ("APINBCO") and $C_{10}H_{18}O_2$ ("APINBOH") through similar pathways.[156] All three OVOC2 factors contain $NH_4^+ \cdot C_{10}H_{14}O$, though its relative abundance is lower in the OH system. While pinonaldehyde ($C_{10}H_{16}O_2$) is known to undergo dehydration to form $C_{10}H_{14}O$ in H_3O^+ PTR-MS instruments,[175–177] separate measurements of a pinonaldehyde standard using NH_4^+ Vocus show that this dehydration product is much less prominent. Specifically, NH_4^+-adduct signals for $C_{10}H_{14}O$ were more than 250 times weaker than those for $C_{10}H_{16}O_2$ ($NH_4^+ \cdot C_{10}H_{14}O$: $NH_4^+ \cdot C_{10}H_{16}O_2$ = 0.0038; Fig. S5). In contrast, H_3O^+ Vocus measurements of the same standard showed a much higher relative abundance of $C_{10}H_{14}O$ ($H^+ \cdot C_{10}H_{14}O$: $H^+ \cdot C_{10}H_{16}O_2$ = 0.47), consistent with known dehydration artifacts during proton-transfer ionization. This suggests that $NH_4^+ \cdot C_{10}H_{14}O$ represents something else.

Given the greater complexity of the OVOC3 and SOA factors, Fig. 8 summarizes their composition, grouped by carbon and oxygen number, with OVOC2 factors included for reference. Solid bars denote non-halogenated species, vertically striped bars represent chlorinated species, and diagonally striped bars denote brominated species. Several trends are evident:

1. Carbon oxidation state increases in the order Br < Cl < OH across all systems.

2. Within each system, OVOC3 and SOA factors are more oxidized than the OVOC2 factor.

3. Carbon number distributions are broader and more complex for OH and Cl systems than for Br, suggesting more extensive fragmentation and multigenerational oxidative aging.

4. The fraction of halogenated species, shown in the pie chart insets of Fig. 8d–i, increased in the order SOA < OVOC2 <

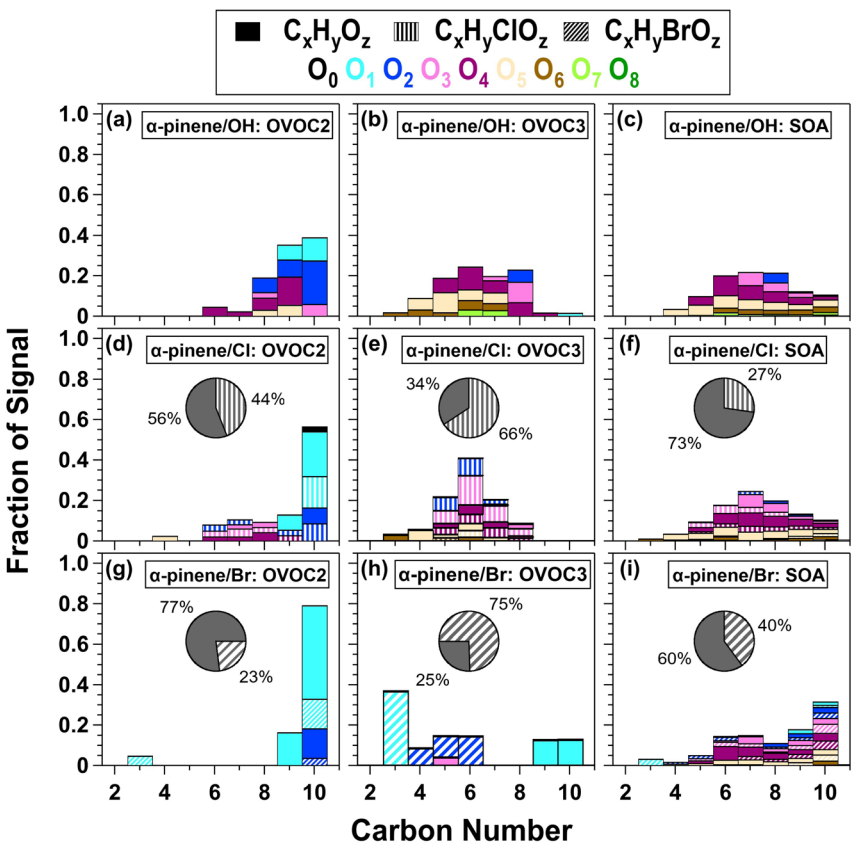

Fig. 8 Carbon number distributions for OVOC2, OVOC3, and SOA factors resulting from oxidation of α-pinene by (a–c) OH, (d–f) Cl, and (g–i) Br. Fill patterns distinguish non-halogenated ($C_xH_yO_z$, solid), chlorinated ($C_xH_yClO_z$, vertical stripes), and brominated ($C_xH_yBrO_z$, diagonal stripes) compounds, while the colors indicate the number of oxygen atoms. Pie charts in the halogen experiments quantify the total contribution of halogenated products to each fraction.

OVOC3 for Cl and OVOC2 < SOA < OVOC3 for Br. These trends suggest that Cl and Br atoms are more likely retained in gas-phase products than in lower-volatility species that contribute to SOA.

5. Br-SOA contained a higher fraction of halogenated signals than Cl-SOA, which is qualitatively consistent with previous findings from α-pinene ozonolysis SOA exposed to Cl and Br.[126]These trends are complicated by potential HCl and HBr elimination *via* chemical processes in the OFR and/or thermal degradation in the VIA, making quantitative interpretation uncertain. Nonetheless, the enrichment of halogenated signals in the OVOC3 factors combined with lower levels of halogenated signals in the SOA factors supports the idea that Cl and Br are preferentially retained in more volatile fragmentation products.

Differences in OVOC and SOA composition among the α-pinene/OH, α-pinene/Cl, and α-pinene/Br systems are linked to differences in the fate of RO_2 formed from OH, Cl and Br oxidation. Fig. 9 shows F_{RO_2} in the absence of isomerization/autooxidation. In the OH system, RO_2 loss is dominated by reactions with HO_2 and OH: $F_{RO_2+HO_2}$ decreased from 0.96 to 0.73 and F_{RO_2+OH} increased from 0.02 to 0.27 with rising OH_{exp} (Fig. 9a). In contrast, RO_2 produced from Cl and Br oxidation show more complex RO_2 fates. In the α-pinene/Cl system (Fig. 9b), $F_{RO_2+RO_2}$ decreases from 0.50 to 0.11, $F_{RO_2+HO_2}$ decreases from 0.36 to 0.22, F_{RO_2+Cl} increases from 0.08 to 0.37, and F_{RO_2+ClO} rises from 0.06 to 0.30. In the α-pinene/Br system (Fig. 9c), $F_{RO_2+RO_2}$ drops from 0.23 to 0.002, $F_{RO_2+HO_2}$ decreases from 0.23 to 0.05, F_{RO_2+Br} increases from 0.30 to 0.90, and F_{RO_2+BrO} decreases from 0.24 to 0.05. To assess the role of RO_2 isomerization/autooxidation, we ran separate simulations assuming isomerization rate coefficients (k_{isom}) of 0.1, 1, and 4 s^{-1} (Fig. S6–S8). These values span the range of experimentally observed rates,[163] with k_{isom} = 4 s^{-1} corresponding to the isomerization rate coefficient of the "APINCO2" peroxy radical[156,165] derived from H-abstraction on α-pinene's terminal methyl group. In the α-pinene/OH system, RO_2 loss remains dominated by RO_2 + HO_2 reactions at k_{isom} = 0.1 s^{-1}. Isomerization becomes competitive with RO_2 + HO_2 at k_{isom} = 1 s^{-1} and becomes dominant at k_{isom} = 4 s^{-1}. In the α-pinene/Cl system, isomerization is competitive with RO_2 + Cl at k_{isom} = 0.1 s^{-1} and becomes dominant at $k_{isom} \geq 1$ s^{-1}. Finally, in the α-pinene/Br system, RO_2 + Br remains dominant at k_{isom} = 0.1 s^{-1} and under most k_{isom} = 1 s^{-1} conditions. However, isomerization plays an important role at k_{isom} = 1 s^{-1} and becomes dominant at k_{isom} = 4 s^{-1}. In summary, while exact contributions are uncertain, this analysis suggests that RO_2 + HO_2 reactions dominate in the α-pinene/OH system, multiple pathways (including RO_2 + Cl and isomerization) are important in the α-pinene/Cl system, and RO_2 + Br reactions dominate in the α-pinene/Br system, with increasing isomerization at higher at higher k_{isom} values. These mechanistic differences contribute to the observed variability in product distributions and SOA formation across the three oxidant systems.

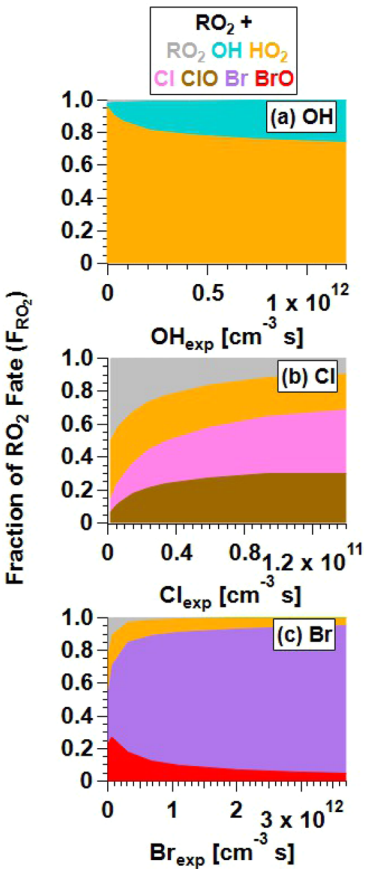

Fig. 9 Modeled fates of the organic peroxy radical (RO_2) as a function of oxidant exposure during the (a) OH, (b) Cl, and (c) Br oxidation of α-pinene in the absence of isomerization/autooxidation reactions. Reactions and kinetic rate coefficients used in these calculations are provided in Table S2.

4 Conclusions

In this study, we presented a comprehensive laboratory investigation into the gas and condensed-phase products generated from the oxidation of α-pinene by OH, Cl, and Br. By employing a Vocus equipped with a VIA and NH_4^+ reagent ion chemistry, we characterized a wide array of oxidation products, including multifunctional organic compounds and previously challenging-to-measure low-volatility species, using a single reagent ion. PMF analysis revealed consistent formation of four distinct factors corresponding to early-generation VOCs/OVOCs, later-generation oxidized products, and low-volatility species contributing to SOA.

Our results demonstrate distinct chemical pathways and product distributions for each oxidant. While the initial oxidation of α-pinene by all three oxidants yielded $C_{10}H_{14,16}O$ and $C_{10}H_{16}O_2$ products, among others, subsequent reactions led to significantly different compound classes. OH-initiated oxidation produced a complex mixture of OVOC and SOA components that were consistent with established α-pinene/OH chemistry. In contrast, α-pinene reactions with Cl and Br atoms led to the formation of a substantial number of halogenated organic compounds. Key early-generation gas-phase products identified included $C_{10}H_{15}ClO$, and $C_{10}H_{15}ClO_2$ from the Cl reaction, and $C_{10}H_{15}BrO$ and $C_{10}H_{15}BrO_2$ from the Br reaction.

The product mass spectra obtained for each oxidation system provide unique fingerprints that can aid in identifying the chemical history and sources of ambient organic aerosol. Cl- and Br-initiated oxidation produced condensed-phase products that were generally less oxidized than those from OH oxidation, with Br-SOA being the least oxidized overall. However, Br-SOA retained a higher fraction of halogenated products than Cl-SOA. Photochemical modeling demonstrated oxidant-specific differences in RO_2 fate, with RO_2 + HO_2 reactions dominating under OH oxidation, a more complex interplay of reactions under Cl oxidation, and RO_2 + Br reactions dominating under Br oxidation. These differences help explain the observed variation in SOA composition and oxidative aging between systems.

Altogether, these results underscore that oxidation by halogen atoms leads to distinct chemical pathways and product distributions compared to OH oxidation. This highlights the need for updated chemical mechanisms and SOA yield treatments that explicitly account for Cl- and Br-mediated oxidation chemistry, especially in regions where halogen atoms are abundant. The presence of these species may alter the physicochemical properties of atmospheric aerosols, including their hygroscopicity, optical properties, and potential toxicity, particularly in marine and coastal environments, with important implications for air quality, climate, and human health. This work highlights the power and utility of NH_4^+ CIMS as a tool for elucidating complex atmospheric oxidation mechanisms, from initial gas-phase reactions to the formation and chemical evolution of aerosols. Future studies should focus on extending this methodology to other precursors and exploring the evolution of these distinct SOA types under a broader range of atmospheric conditions to better constrain their impact in regional and global models.

Author contributions

AL and JK conceived, planned, and carried out the experiments. AL performed data analysis. AL, MC, AA, MA and ND contributed to the interpretation of the results. AL took the lead in writing the manuscript. All authors provided feedback on the manuscript.

Conflicts of interest

There are no conflicts to declare.

Data availability

Data for this article, including source files used to generate Fig. 1 and 3–9, are available at Open Science Framework at [https://osf.io/6fc3q/overview].

Supplementary information (SI): additional experimental time series, molecular formula assignments and proposed structures, Van Krevelen analyses of α-pinene Cl-SOA and Br-SOA composition, data obtained from Vocus measurements of pinonaldehyde, and detailed chemical mechanisms and kinetic parameters used in the OFR modeling. See DOI: https://doi.org/10.1039/d5ea00091b.

Acknowledgements

This work was supported by the Atmospheric Chemistry Program of the United States National Science Foundation: grant AGS-1934352 to Aerodyne Research. AL thanks Lea Hildebrandt Ruiz (University of Texas at Austin) and Harald Stark (Aerodyne Research) for helpful discussions.

References

1 X. Wang, D. J. Jacob, S. D. Eastham, M. P. Sulprizio, L. Zhu, Q. Chen, B. Alexander, T. Sherwen, M. J. Evans, B. H. Lee, J. D. Haskins, F. D. Lopez-Hilfiker, J. A. Thornton, G. L. Huey and H. Liao, *Atmos. Chem. Phys.*, 2019, **19**, 3981–4003.
2 X. Peng, W. Wang, M. Xia, H. Chen, A. R. Ravishankara, Q. Li, A. Saiz-Lopez, P. Liu, F. Zhang, C. Zhang, L. Xue, X. Wang, C. George, J. Wang, Y. Mu, J. Chen and T. Wang, *Natl. Sci. Rev.*, 2020, **8**, nwaa304.
3 A. K. Baker, C. Sauvage, U. R. Thorenz, P. van Velthoven, D. E. Oram, A. Zahn, C. A. M. Brenninkmeijer and J. Williams, *Sci. Rep.*, 2016, **6**, 36821.
4 X. Yi, G. Sarwar, J. Bian, L. Huang, Q. Li, S. Jiang, H. Liu, Y. Wang, H. Chen, T. Wang, J. Chen, A. Saiz-Lopez, D. C. Wong and L. Li, *J. Geophys. Res. Atmos.*, 2023, **128**, e2023JD038898.
5 G. Chen, Z. Chen, Y. Zhang, X. Fan, L. Xu, Z. Lin, X. Ji and J. Chen, *npj Clim. Atmos. Sci.*, 2025, **8**, 248.
6 P. L. Tanaka, D. D. Riemer, S. Chang, G. Yarwood, E. C. McDonald-Buller, E. C. Apel, J. J. Orlando, P. J. Silva, J. L. Jimenez, M. R. Canagaratna, J. D. Neece, C. Mullins and D. T. Allen, *Atmos. Environ.*, 2003, **37**, 1393–1400.
7 C. B. Faxon and D. T. Allen, *Environ. Chem.*, 2013, **10**, 221–233.
8 C. G. Masoud, M. Modi, N. Bhattacharyya, L. G. Jahn, K. N. McPherson, P. Abue, K. Patel, D. T. Allen and L. Hildebrandt Ruiz, *Environ. Sci. Technol.*, 2023, **57**, 15454–15464.
9 D. Chang, Q. Li, Z. Wang, J. Dai, X. Fu, J. Guo, L. Zhu, D. Pu, C. A. Cuevas, R. P. Fernandez, W. Wang, M. Ge, J. C. H. Fung, A. K. H. Lau, C. Granier, G. Brasseur, A. Pozzer, A. Saiz-Lopez, Y. Song and T. Wang, *Natl. Sci. Rev.*, 2024, **11**, nwae285.
10 W. R. Simpson, R. von Glasow, K. Riedel, P. Anderson, P. Ariya, J. Bottenheim, J. Burrows, L. J. Carpenter, U. Frieß, M. E. Goodsite, D. Heard, M. Hutterli, H.-W. Jacobi, L. Kaleschke, B. Neff, J. Plane, U. Platt, A. Richter, H. Roscoe, R. Sander, P. Shepson, J. Sodeau, A. Steffen, T. Wagner and E. Wolff, *Atmos. Chem. Phys.*, 2007, **7**, 4375–4418.
11 C. R. Thompson, P. B. Shepson, J. Liao, L. G. Huey, C. Cantrell, F. Flocke and J. Orlando, *Atmos. Chem. Phys.*, 2017, **17**, 3401–3421.
12 S. Wang, S. M. McNamara, C. W. Moore, D. Obrist, A. Steffen, P. B. Shepson, R. M. Staebler, A. R. W. Raso and K. A. Pratt, *Proc. Natl. Acad. Sci. U. S. A.*, 2019, **116**, 14479–14484.

13 J. H. Knox and R. L. Nelson, *Trans. Faraday Soc.*, 1959, **55**, 937–946.
14 K. C. Ferguson and E. Whittle, *Trans. Faraday Soc.*, 1971, **67**, 2618–2628.
15 K. H. Homann, *Ber. Bunsenges. Phys. Chem.*, 1973, **77**, 223–224.
16 D. L. Baulch, J. Duxbury, S. J. Grant and D. C. Montague, *J. Phys. Chem. Ref. Data*, 1981, **10**, Suppl. No. 1.
17 T. Ohta, *Int. J. Chem. Kinet.*, 1984, **16**, 879–886.
18 D. H. Semmes, A. R. Ravishankara, C. A. Gump-Perkins and P. H. Wine, *Int. J. Chem. Kinet.*, 1985, **17**, 303–313.
19 R. Atkinson, *Chem. Rev.*, 1986, **86**, 69–201.
20 S. W. Benson, O. Kondo and R. M. Marshall, *Int. J. Chem. Kinet.*, 1987, **19**, 829–839.
21 R. Atkinson and S. M. Aschmann, *J. Phys. Chem.*, 1988, **92**, 4008.
22 F. Nolting, W. Behnke and C. Zetzsch, *J. Atmos. Chem.*, 1988, **6**, 47–59.
23 J. J. Russell, J. A. Seetula and D. Gutman, *J. Am. Chem. Soc.*, 1988, **110**, 3092–3099.
24 T. J. Wallington, L. M. Skewes, W. O. Siegl, C.-H. Wu and S. M. Japar, *Int. J. Chem. Kinet.*, 1988, **20**, 867–875.
25 R. Atkinson and S. M. Aschmann, *Int. J. Chem. Kinet.*, 1989, **21**, 355–365.
26 I. Barnes, V. Bastian, K. H. Becker, R. Overath and Z. Tong, *Int. J. Chem. Kinet.*, 1989, **21**, 499–517.
27 T. J. Wallington, L. M. Skewes, W. O. Siegl and S. M. Japar, *Int. J. Chem. Kinet.*, 1989, **21**, 1069–1076.
28 L. Nelson, O. Rattigan, R. Neavyn, H. Sidebottom, J. Treacy and O. J. Nielsen, *Int. J. Chem. Kinet.*, 1990, **22**, 1111–1126.
29 O. J. Nielsen, H. W. Sidebottom, L. Nelson, O. Rattigan, J. J. Treacy and D. J. O'Farrell, *Int. J. Chem. Kinet.*, 1990, **22**, 603–612.
30 R. Atkinson, D. L. Baulch, R. A. Cox, J. Hampson, R. F., J. A. Kerr and J. Troe, *J. Phys. Chem. Ref. Data*, 1992, **21**, 1125–1568.
31 D. L. Baulch, C. J. Cobos, R. A. Cox, C. Esser, P. Frank, T. Just, J. A. Kerr, M. J. Pilling, J. Troe, R. W. Walker and J. Warnatz, *J. Phys. Chem. Ref. Data*, 1992, **21**, 411.
32 A. Bierbach, I. Barnes and K. Becker, *Atmos. Environ. Gen. Top*, 1992, **26**, 813–817.
33 D. M. Rowley, R. Lesclaux, P. D. Lightfoot, B. Noziere, T. J. Wallington and M. D. Hurley, *J. Phys. Chem.*, 1992, **96**, 4889–4894.
34 B. Noziere, R. Lesclaux, M. D. Hurley, M. A. Dearth and T. J. Wallington, *J. Phys. Chem.*, 1994, **98**, 2864–2873.
35 S. M. Aschmann and R. Atkinson, *Int. J. Chem. Kinet.*, 1995, **27**, 613–622.
36 A. Bierbach, I. Barnes and K. Becker, *Atmos. Environ.*, 1995, **29**, 2651–2660.
37 A. Bierbach, I. Barnes and K. H. Becker, *Int. J. Chem. Kinet.*, 1996, **28**, 565–577.
38 P. A. Hooshiyar and H. Niki, *Int. J. Chem. Kinet.*, 1995, **27**, 1197–1206.
39 E. W. Kaiser and T. J. Wallington, *J. Phys. Chem.*, 1996, **100**, 4111–4119.
40 D. J. Kinnison, W. Mengon and J. A. Kerr, *J. Chem. Soc., Faraday Trans.*, 1996, **92**, 369–372.
41 S. Teton, A. Mellouki, G. Le Bras and H. Sidebottom, *Int. J. Chem. Kinet.*, 1996, **28**, 291–297.
42 A. A. Turnipseed, S. B. Barone and A. R. Ravishankara, *J. Phys. Chem.*, 1996, **100**, 14703–14713.
43 R. Atkinson, D. L. Baulch, R. A. Cox, R. F. Hampson, J. A. Kerr, M. J. Rossi and J. Troe, *J. Phys. Chem. Ref. Data*, 1997, **26**, 521–1011.
44 W. B. DeMore, S. P. Sander, D. M. Golden, R. F. Hampson, M. J. Kurylo, C. J. Howard, A. R. Ravishankara, C. E. Kolb, M. J. Molina, *Chemical Kinetics and Photochemical Data for Use in Stratospheric Modeling*, JPL Publication 97-4, 1997.
45 M. L. Ragains and B. J. Finlayson-Pitts, *J. Phys. Chem. A*, 1997, **101**, 1509–1517.
46 J. Shi and M. J. Bernhard, *Int. J. Chem. Kinet.*, 1997, **29**, 349–358.
47 G. S. Tyndall, J. J. Orlando, T. J. Wallington, M. Dill and E. W. Kaiser, *Int. J. Chem. Kinet.*, 1997, **29**, 43–55.
48 J. T. Jodkowski, M.-T. Rayez, J.-C. Rayez, T. Bérces and S. Dóbé, *J. Phys. Chem. A*, 1998, **102**, 9230–9243.
49 S. Le Calvé, D. Hitier, G. Le Bras and A. Mellouki, *J. Phys. Chem. A*, 1998, **102**, 4579–4584.
50 B. Nozière and I. Barnes, *J. Geophys. Res. Atmos.*, 1998, **103**, 25587–25597.
51 I. Szilágyi, K. Imrik, S. Dóbé and T. Bérces, *Ber. Bunsenges. Phys. Chem.*, 1998, **102**, 79–84.
52 A. Bierbach, I. Barnes and K. Becker, *Atmos. Environ.*, 1999, **33**, 2981–2992.
53 B. J. Finlayson-Pitts, C. J. Keoshian, B. Buehler and A. A. Ezell, *Int. J. Chem. Kinet.*, 1999, **31**, 491–499.
54 T. Maurer, I. Barnes and K. H. Becker, *Int. J. Chem. Kinet.*, 1999, **31**, 883–893.
55 C. Sauer, I. Barnes and K. Becker, *Atmos. Environ.*, 1999, **33**, 2969–2979.
56 R. Atkinson, E. C. Tuazon and S. M. Aschmann, *Environ. Sci. Technol.*, 2000, **34**, 623–631.
57 B. Ramacher, J. J. Orlando and G. S. Tyndall, *Int. J. Chem. Kinet.*, 2000, **32**, 460–465.
58 R. Thévenet, A. Mellouki and G. Le Bras, *Int. J. Chem. Kinet.*, 2000, **32**, 676–685.
59 R. Atkinson, D. Baulch, R. Cox, J. Crowley, J. Hampson, R. F., J. Kerr, M. Rossi and J. Troe, *IUPAC Subcommittee on Gas Kinetic Data Evaluation for Atmospheric Chemistry - Web Version*, 2001.
60 W. R. Bradley, S. E. Wyatt, J. R. Wells, M. V. Henley and G. M. Graziano, *Int. J. Chem. Kinet.*, 2001, **33**, 108–117.
61 J. Albaladejo, B. Ballesteros, E. Jiménez, P. Martín and E. Martínez, *Atmos. Environ.*, 2002, **36**, 3231–3239.
62 M. J. Ezell, W. Wang, A. A. Ezell, G. Soskin and B. J. Finlayson-Pitts, *Phys. Chem. Chem. Phys.*, 2002, **4**, 5813–5820.
63 K. J. Gill and R. A. Hites, *J. Phys. Chem. A*, 2002, **106**, 2538–2544.
64 W. Wang, M. J. Ezell, A. A. Ezell, G. Soskin and B. J. Finlayson-Pitts, *Phys. Chem. Chem. Phys.*, 2002, **4**, 1824–1831.

65 R. Atkinson, *Atmos. Chem. Phys. Discuss.*, 2003, **3**, 2233–2307.
66 M. D. Hurley, W. F. Schneider, T. J. Wallington, D. J. Mann, J. D. DeSain and C. A. Taatjes, *J. Phys. Chem. A*, 2003, **107**, 2003–2010.
67 J. Moriarty, H. Sidebottom, J. Wenger, A. Mellouki and G. Le Bras, *J. Phys. Chem. A*, 2003, **107**, 1499–1505.
68 J. J. Orlando, G. S. Tyndall, E. C. Apel, D. D. Riemer and S. E. Paulson, *Int. J. Chem. Kinet.*, 2003, **35**, 334–353.
69 R. Atkinson, D. L. Baulch, R. A. Cox, J. N. Crowley, R. F. Hampson, R. G. Hynes, M. E. Jenkin, M. J. Rossi and J. Troe, *Atmos. Chem. Phys.*, 2004, **4**, 1461–1738.
70 C. A. Cuevas, A. Notario, E. Martínez and J. Albaladejo, *Phys. Chem. Chem. Phys.*, 2004, **6**, 2230–2236.
71 T. Imamura, Y. Iida, K. Obi, I. Nagatani, K. Nakagawa, I. Patroescu-Klotz and S. Hatakeyama, *Int. J. Chem. Kinet.*, 2004, **36**, 379–385.
72 B. Caba nas, F. Villanueva, P. Martín, M. Baeza, S. Salgado and E. Jiménez, *Atmos. Environ.*, 2005, **39**, 1935–1944.
73 E. Jiménez, B. Ballesteros, E. Martínez and J. Albaladejo, *Environ. Sci. Technol.*, 2005, **39**, 814–820.
74 D. Rodríguez, A. Rodríguez, A. Notario, A. Aranda, Y. Díaz-de Mera and E. Martínez, *Atmos. Chem. Phys.*, 2005, **5**, 3433–3440.
75 C. A. Cuevas, A. Notario, E. Martínez and J. Albaladejo, *Atmos. Environ.*, 2006, **40**, 3845–3854.
76 R. S. Anderson, L. Huang, R. Iannone and J. Rudolph, *J. Phys. Chem. A*, 2007, **111**, 495–504.
77 M. Baasandorj and P. S. Stevens, *J. Phys. Chem. A*, 2007, **111**, 640–649.
78 B. Ballesteros, A. Garzón, E. Jiménez, A. Notario and J. Albaladejo, *Phys. Chem. Chem. Phys.*, 2007, **9**, 1210–1218.
79 M. E. Davis, R. K. Talukdar, G. Notte, G. B. Ellison and J. B. Burkholder, *Environ. Sci. Technol.*, 2007, **41**, 3959–3965.
80 E. Jiménez, B. Lanza, E. Martínez and J. Albaladejo, *Atmos. Chem. Phys.*, 2007, **7**, 1565–1574.
81 B. Caba nas, A. Tapia, F. Villanueva, S. Salgado, E. Monedero and P. Martín, *Int. J. Chem. Kinet.*, 2008, **40**, 670–678.
82 P. M. Cometto, P. R. Dalmasso, R. A. Taccone, S. I. Lane, F. Oussar, V. Daële, A. Mellouki and G. L. Bras, *J. Phys. Chem. A*, 2008, **112**, 4444–4450.
83 D. Rodriguez, A. Rodriguez, A. Soto, A. Aranda, Y. Diaz-de Mera and A. Notario, *J. Atmos. Chem.*, 2008, **59**, 187–197.
84 B. R. Giri and J. M. Roscoe, *J. Phys. Chem. A*, 2009, **113**, 8001–8010.
85 G. Oksdath-Mansilla, A. B. Pe né nory, M. Albu, I. Barnes, P. Wiesen and M. A. Teruel, *Chem. Phys. Lett.*, 2009, **477**, 22–27.
86 R. Sivaramakrishnan and J. V. Michael, *J. Phys. Chem. A*, 2009, **113**, 5047–5060.
87 B. R. Giri and J. M. Roscoe, *J. Phys. Chem. A*, 2010, **114**, 8369–8375.
88 M. E. Jenkin, M. D. Hurley and T. J. Wallington, *J. Phys. Chem. A*, 2010, **114**, 408–416.
89 E. W. Kaiser, T. J. Wallington and M. D. Hurley, *J. Phys. Chem. A*, 2010, **114**, 343–354.
90 S. M. Aschmann, J. Arey and R. Atkinson, *J. Phys. Chem. A*, 2011, **115**, 14452–14461.
91 M. E. Davis and J. B. Burkholder, *Atmos. Chem. Phys.*, 2011, **11**, 3347–3358.
92 Y. Gai, M. Ge and W. Wang, *Atmos. Environ.*, 2011, **45**, 53–59.
93 A. A. Ceacero-Vega, B. Ballesteros, I. Bejan, I. Barnes, E. Jiménez and J. Albaladejo, *J. Phys. Chem. A*, 2012, **116**, 4097–4107.
94 L. Renbaum-Wolff and G. D. Smith, *J. Phys. Chem. A*, 2012, **116**, 6664–6674.
95 D. Rodríguez, A. Rodríguez, A. Garzón, J. M. Granadino-Roldán, A. Soto, A. Aranda and A. N., *Mol. Phys.*, 2012, **110**, 2941–2950.
96 E. Szabo, G. L. Zuegner, M. Farkas, I. Szilagyi and S. Dobe, *Oxid. Commun.*, 2012, **35**, 538–544.
97 S. M. Aschmann and R. Atkinson, *Int. J. Chem. Kinet.*, 2013, **45**, 52–58.
98 R. G. Gibilisco, A. N. Santiago and M. A. Teruel, *Atmos. Environ.*, 2013, **77**, 358–364.
99 J. A. Liljegren and P. S. Stevens, *Int. J. Chem. Kinet.*, 2013, **45**, 787–794.
100 M. R. Dash and B. Rajakumar, *Atmos. Environ.*, 2014, **99**, 183–195.
101 R. G. Gibilisco, I. Bejan, I. Barnes, P. Wiesen and M. A. Teruel, *Atmos. Environ.*, 2014, **94**, 564–572.
102 M. Riva, R. M. Healy, P.-M. Flaud, E. Perraudin, J. C. Wenger and E. Villenave, *J. Phys. Chem. A*, 2014, **118**, 3535–3540.
103 A. Lauraguais, I. Bejan, I. Barnes, P. Wiesen, C. Coeur-Tourneur and A. Cassez, *J. Phys. Chem. A*, 2014, **118**, 1777–1784.
104 R. G. Gibilisco, M. B. Blanco, I. Bejan, I. Barnes, P. Wiesen and M. A. Teruel, *Environ. Sci. Technol.*, 2015, **49**, 7717–7725.
105 A. Lauraguais, I. Bejan, I. Barnes, P. Wiesen and C. Coeur, *J. Phys. Chem. A*, 2015, **119**, 6179–6187.
106 A. Safron, M. Strandell, A. Kierkegaard and M. Macleod, *Int. J. Chem. Kinet.*, 2015, **47**, 420–428.
107 B. Srinivasulu and G. Rajakumar, *J. Chem. Sci.*, 2016, **128**, 977–989.
108 S. Ausmeel, C. Andersen, O. J. Nielsen, F. F. Østerstrøm, M. S. Johnson and E. J. K. Nilsson, *J. Phys. Chem. A*, 2017, **121**, 4123–4131.
109 J. A. Barrera, P. R. Dalmasso, R. A. Taccone and S. I. Lane, *Environ. Sci. Pollut. Res.*, 2017, **24**, 26049–26059.
110 J. A. Barrera, M. de los, A. Garavagno, P. R. Dalmasso and R. A. Taccone, *Atmos. Environ.*, 2019, **202**, 28–40.
111 B. Shi, W. Wang, L. Zhou, J. Li, J. Wang, Y. Chen, W. Zhang and M. Ge, *Atmos. Environ.*, 2019, **207**, 75–81.
112 M. W. Alton and E. C. Browne, *Environ. Sci. Technol.*, 2020, **54**, 5992–5999.
113 I. Colmenar, S. Salgado, P. Martín, I. Aranda, A. Tapia and B. Caba nas, *Atmos. Environ.*, 2020, **224**, 117367.
114 K. H. Møller, R. V. Otkjær, J. Chen and H. G. Kjaergaard, *J. Phys. Chem. A*, 2020, **124**, 2885–2896.

115 J. T. Shaw, A. R. Rickard, M. J. Newland and T. J. Dillon, *Atmos. Chem. Phys.*, 2020, **20**, 9725–9736.
116 S. Szymański and D. S. Sarzyński, *Int. J. Chem. Kinet.*, 2020, **52**, 957–963.
117 Z. Tan, L. Hantschke, M. Kaminski, I.-H. Acir, B. Bohn, C. Cho, H.-P. Dorn, X. Li, A. Novelli, S. Nehr, F. Rohrer, R. Tillmann, R. Wegener, A. Hofzumahaus, A. Kiendler-Scharr, A. Wahner and H. Fuchs, *Atmos. Chem. Phys.*, 2021, **21**, 16067–16091.
118 A. Allani and M. N. Romanias, *Int. J. Chem. Kinet.*, 2022, **54**, 424–434.
119 M. Asensio, M. Anti nolo, S. Blázquez, J. Albaladejo and E. Jiménez, *Atmos. Chem. Phys.*, 2022, **22**, 2689–2701.
120 D. Van Hoomissen, A. Chattopadhyay and J. B. Burkholder, *Int. J. Chem. Kinet.*, 2025, **57**, 213–231.
121 Q. K. Timerghazin and P. A. Ariya, *Phys. Chem. Chem. Phys.*, 2001, **3**, 3981–3986.
122 X. Cai and R. J. Griffin, *J. Geophys. Res.*, 2006, **111**, D14206.
123 Y. Wang, M. Riva, H. Xie, L. Heikkinen, S. Schallhart, Q. Zha, C. Yan, X.-C. He, O. Peräkylä and M. Ehn, *Atmos. Chem. Phys.*, 2020, **20**, 5145–5155.
124 C. G. Masoud and L. Hildebrandt Ruiz, *ACS Earth Space Chem.*, 2021, **5**, 2307–2319.
125 A. T. Lambe, A. M. Avery, N. Bhattacharyya, D. S. Wang, M. Modi, C. G. Masoud, L. H. Ruiz and W. H. Brune, *Environ. Sci.: Atmos.*, 2022, **2**, 687–701.
126 J. Ofner, N. Balzer, J. Buxmann, H. Grothe, P. Schmitt-Kopplin, U. Platt and C. Zetzsch, *Atmos. Chem. Phys.*, 2012, **12**, 5787–5806.
127 Q. Li, X. Fu, X. Peng, W. Wang, A. Badia, R. P. Fernandez, C. A. Cuevas, Y. Mu, J. Chen, J. L. Jimenez, T. Wang and A. Saiz-Lopez, *Environ. Sci. Technol.*, 2021, **55**, 13625–13637.
128 B. L. Deming, D. Pagonis, X. Liu, D. A. Day, R. Talukdar, J. E. Krechmer, J. A. de Gouw, J. L. Jimenez and P. J. Ziemann, *Atmos. Meas. Tech.*, 2019, **12**, 3453–3461.
129 A. T. Lambe, J. E. Krechmer, Z. Peng, J. R. Casar, A. J. Carrasquillo, J. D. Raff, J. L. Jimenez and D. R. Worsnop, *Atmos. Meas. Tech.*, 2019, **12**, 299–311.
130 J. P. Rowe, A. T. Lambe and W. H. Brune, *Atmos. Chem. Phys.*, 2020, **20**, 13417–13424.
131 J. Mao, X. Ren, W. Brune, J. Olson, J. Crawford, A. Fried, L. Huey, R. Cohen, B. Heikes and H. Singh, *Atmos. Chem. Phys.*, 2009, **9**, 163–173.
132 A. V. Baklanov and L. N. Krasnoperov, *J. Phys. Chem. A*, 2001, **105**, 97–103.
133 B. Ghosh, D. K. Papanastasiou and J. B. Burkholder, *J. Chem. Phys.*, 2012, **137**, 164315.
134 C.-C. Wu, H.-C. Lin, Y.-B. Chang, P.-Y. Tsai, Y.-Y. Yeh, H. Fan, K.-C. Lin and J. S. Francisco, *J. Chem. Phys.*, 2011, **135**, 234308.
135 D. Paul, H. K. Kim, M. M. Rahman and T. K. Kim, *J. Appl. Spectrosc.*, 2021, **88**, 737–743.
136 C. R. Stephens, P. B. Shepson, A. Steffen, J. W. Bottenheim, J. Liao, L. G. Huey, E. Apel, A. Weinheimer, S. R. Hall, C. Cantrell, B. C. Sive, D. J. Knapp, D. D. Montzka and R. S. Hornbrook, *J. Geophys. Res.*, 2012, **117**, D14.
137 J. Krechmer, F. Lopez-Hilfiker, A. Koss, M. Hutterli, C. Stoermer, B. Deming, J. Kimmel, C. Warneke, R. Holzinger, J. Jayne, D. Worsnop, K. Fuhrer, M. Gonin and J. de Gouw, *Anal. Chem.*, 2018, **90**, 12011–12018.
138 P. Khare, J. E. Krechmer, J. E. Machesky, T. Hass-Mitchell, C. Cao, J. Wang, F. Majluf, F. Lopez-Hilfiker, S. Malek, W. Wang, K. Seltzer, H. O. T. Pye, R. Commane, B. C. McDonald, R. Toledo-Crow, J. E. Mak and D. R. Gentner, *Atmos. Chem. Phys.*, 2022, **22**, 14377–14399.
139 L. Xu, M. M. Coggon, C. E. Stockwell, J. B. Gilman, M. A. Robinson, M. Breitenlechner, A. Lamplugh, J. D. Crounse, P. O. Wennberg, J. A. Neuman, G. A. Novak, P. R. Veres, S. S. Brown and C. Warneke, *Atmos. Meas. Tech.*, 2022, **15**, 7353–7373.
140 E. Häkkinen, J. Zhao, F. Graeffe, N. Fauré, J. Krechmer, D. Worsnop, H. Timonen, M. Ehn and J. Kangasluoma, *Atmos. Meas. Tech.*, 2022, **2022**, 1–29.
141 A. M. Avery, M. W. Alton, M. R. Canagaratna, J. E. Krechmer, D. T. Sueper, N. Bhattacharyya, L. Hildebrandt Ruiz, W. H. Brune and A. T. Lambe, *ACS Earth Space Chem.*, 2023, **7**, 218–229.
142 J. Zhao, V. Mickwitz, Y. Luo, E. Häkkinen, F. Graeffe, J. Zhang, H. Timonen, M. Canagaratna, J. E. Krechmer, Q. Zhang, M. Kulmala, J. Kangasluoma, D. Worsnop and M. Ehn, *Atmos. Meas. Tech.*, 2024, **17**, 1527–1543.
143 D. Sueper, 2022, http://cires.colorado.edu/jimenez-group/ToFAMSResources/ToFSoftware.
144 M. R. Canagaratna, J. L. Jimenez, J. H. Kroll, Q. Chen, S. H. Kessler, P. Massoli, L. Hildebrandt Ruiz, E. Fortner, L. R. Williams, K. R. Wilson, J. D. Surratt, N. M. Donahue, J. T. Jayne and D. R. Worsnop, *Atmos. Chem. Phys.*, 2015, **15**, 253–272.
145 H. Stark, R. L. Yatavelli, S. L. Thompson, J. R. Kimmel, M. J. Cubison, P. S. Chhabra, M. R. Canagaratna, J. T. Jayne, D. R. Worsnop and J. L. Jimenez, *Int. J. Mass Spectrom.*, 2015, **389**, 26–38.
146 P. Paatero and U. Tapper, *Environmetrics*, 1994, **5**, 111–126.
147 C. Yan, W. Nie, M. Äijälä, M. P. Rissanen, M. R. Canagaratna, P. Massoli, H. Junninen, T. Jokinen, N. Sarnela, S. A. K. Häme, S. Schobesberger, F. Canonaco, L. Yao, A. S. H. Prévôt, T. Petäjä, M. Kulmala, M. Sipilä, D. R. Worsnop and M. Ehn, *Atmos. Chem. Phys.*, 2016, **16**, 12715–12731.
148 I. Ulbrich, M. Canagaratna, Q. Zhang, D. Worsnop and J. Jimenez, *Atmos. Chem. Phys.*, 2009, **9**, 2891–2918.
149 N. M. Donahue, S. A. Epstein, S. N. Pandis and A. L. Robinson, *Atmos. Chem. Phys.*, 2011, **11**, 3303–3318.
150 Z. Peng and J. L. Jimenez, *J. Chem. Educ.*, 2019, **96**, 806–811.
151 R. Li, B. B. Palm, A. M. Ortega, J. Hlywiak, W. Hu, Z. Peng, D. A. Day, C. Knote, W. H. Brune, J. A. De Gouw and J. L. Jimenez, *J. Phys. Chem. A*, 2015, **119**, 150406123535006.
152 Z. Peng and J. L. Jimenez, *Chem. Soc. Rev.*, 2020, **49**, 2570–2616.
153 Z. Peng, J. Lee-Taylor, J. J. Orlando, G. S. Tyndall and J. L. Jimenez, *Atmos. Chem. Phys.*, 2019, **19**, 813–834.
154 A. T. Lambe, C. K. Glenn, A. M. Avery, T. Xu, J. C. Ditto, M. R. Canagaratna, D. R. Gentner, K. S. Docherty,

M. Jaoui, J. Zaks, A. K. Bertram, N. L. Ng and P. Liu, *ACS Earth Space Chem.*, 2025, **9**(3), 545–559.
155 W. Tsang and R. F. Hampson, *J. Phys. Chem. Ref. Data*, 1986, **15**, 1087–1279.
156 M. Jenkin, S. Saunders and M. Pilling, *Atmos. Environ.*, 1997, **31**, 81–104.
157 J. S. Francisco and J. N. Crowley, *J. Phys. Chem. A*, 2006, **110**, 3778–3784.
158 S. Enami, T. Yamanaka, T. Nakayama, S. Hashimoto, M. Kawasaki, D. E. Shallcross, Y. Nakano and T. Ishiwata, *J. Phys. Chem. A*, 2007, **111**, 3342–3348.
159 D. E. Shallcross, K. E. Leather, A. Bacak, P. Xiao, E. P. F. Lee, M. Ng, D. K. W. Mok, J. M. Dyke, R. Hossaini, M. P. Chipperfield, M. A. H. Khan and C. J. Percival, *J. Phys. Chem. A*, 2015, **119**, 4618–4632.
160 R. Atkinson, D. L. Baulch, R. A. Cox, J. N. Crowley, R. F. Hampson, R. G. Hynes, M. E. Jenkin, M. J. Rossi and J. Troe, *Atmos. Chem. Phys.*, 2007, **7**, 981–1191.
161 P. J. Ziemann and R. Atkinson, *Chem. Soc. Rev.*, 2012, **41**, 6582–6605.
162 J. J. Orlando and G. S. Tyndall, *Chem. Soc. Rev.*, 2012, **41**, 6294–6317.
163 F. Bianchi, T. Kurtén, M. Riva, C. Mohr, M. P. Rissanen, P. Roldin, T. Berndt, J. D. Crounse, P. O. Wennberg, T. F. Mentel, J. Wildt, H. Junninen, T. Jokinen, M. Kulmala, D. R. Worsnop, J. A. Thornton, N. Donahue, H. G. Kjaergaard and M. Ehn, *Chem. Rev.*, 2019, **119**, 3472–3509.
164 C. Fittschen, *Chem. Phys. Lett.*, 2019, **725**, 102–108.
165 L. Xu, K. H. Møller, J. D. Crounse, R. V. Otkjær, H. G. Kjaergaard and P. O. Wennberg, *J. Phys. Chem. A*, 2019, **123**, 1661–1674.
166 Y. Li, U. Pöschl and M. Shiraiwa, *Atmos. Chem. Phys.*, 2016, **16**, 3327–3344.
167 N. C. Eddingsaas, C. L. Loza, L. D. Yee, J. H. Seinfeld and P. O. Wennberg, *Atmos. Chem. Phys.*, 2012, **12**, 6489–6504.
168 M. Claeys, Y. Iinuma, R. Szmigielski, J. D. Surratt, F. Blockhuys, C. Van Alsenoy, O. Böge, B. Sierau, Y. Gómez-González, R. Vermeylen, P. Van der Veken, M. Shahgholi, A. W. H. Chan, H. Herrmann, J. H. Seinfeld and W. Maenhaut, *Environ. Sci. Technol.*, 2009, **43**, 6976–6982.
169 R. Szmigielski, J. D. Surratt, Y. Gómez-González, P. Van der Veken, I. Kourtchev, R. Vermeylen, F. Blockhuys, M. Jaoui, T. E. Kleindienst, M. Lewandowski, J. H. Offenberg, E. O. Edney, J. H. Seinfeld, W. Maenhaut and M. Claeys, *Geophys. Res. Lett.*, 2007, **34**, L24811.
170 L. Müller, M.-C. Reinnig, K. H. Naumann, H. Saathoff, T. F. Mentel, N. M. Donahue and T. Hoffmann, *Atmos. Chem. Phys.*, 2012, **12**, 1483–1496.
171 N. C. Eddingsaas, C. L. Loza, L. D. Yee, M. Chan, K. A. Schilling, P. S. Chhabra, J. H. Seinfeld and P. O. Wennberg, *Atmos. Chem. Phys.*, 2012, **12**, 7413–7427.
172 T. Jokinen, T. Berndt, R. Makkonen, V.-M. Kerminen, H. Junninen, P. Paasonen, F. Stratmann, H. Herrmann, A. B. Guenther, D. R. Worsnop, M. Kulmala, M. Ehn and M. Sipilä, *Proc. Natl. Acad. Sci. U. S. A.*, 2015, **112**, 7123–7128.
173 L. Poulain, A. Tilgner, M. Brüggemann, P. Mettke, L. He, J. Anders, O. Böge, A. Mutzel and H. Herrmann, *J. Geophys. Res. Atmos.*, 2022, **127**, e2021JD036414.
174 H. Luo, Y. Guo, H. Shen, D. D. Huang, Y. Zhang and D. Zhao, *Environ. Sci.: Atmos.*, 2024, **4**, 519–530.
175 A. Wisthaler, N. Jensen, R. Winterhalter, W. Lindinger and J. Hjorth, *Atmos. Environ.*, 2001, **35**, 6181–6191.
176 A. Lee, A. H. Goldstein, J. H. Kroll, N. L. Ng, V. Varutbangkul, R. C. Flagan and J. H. Seinfeld, *J. Geophys. Res. Atmos.*, 2006, **111**, D07302.
177 B. Rosati, R. Teiwes, K. Kristensen, R. Bossi, H. Skov, M. Glasius, H. B. Pedersen and M. Bilde, *Atmos. Environ.*, 2019, **199**, 15–31.

